JETLAG2008 - An Update

Joseph H.W. Lee, Valiant Cheung and Chris Lai

Croucher Laboratory of Environmental Hydraulics
The University of Hong Kong

Technical Note

December 2008

1. INTRODUCTION

In many coastal cities, partially treated wastewater is often discharged into the receiving water through submarine outfall diffusers to minimize environmental impact. In modern outfall designs, the wastewater is typically discharged through risers fitted circumferentially with 2 - 8 horizontal nozzles (Fig. 1). The mixing of this rosette jet group discharge with the ambient flow U_a involves the complicated interaction of coflowing, oblique-flowing, crossflowing, and counter-flowing jets. Recent studies have shown that for typical outfall riser geometries the dynamic interaction of the adjacent jets in a crossflow is insignificant. The mixing of practical diffuser discharges can hence be treated by treating each jet in the rosette as independent, and accounting for only kinematic merging of the buoyant jets (Lai *et al.* 2008).

Fig. 2 shows a round buoyant jet directed into a uniform horizontal cross flow of velocity U_a. Without loss of generality, the ambient current is assumed to flow along the x-axis. The major parameters governing the flow are the jet volume flux $Q_o = V_o \pi D^2/4$, the kinematic momentum flux $M_o = Q_o V_o$, and the specific buoyancy flux $F_o = Q_o \mathsf{g}'_o = Q[(\rho_a - \rho_o)/\rho_a]\mathsf{g}$, where V_o, ρ_o are jet discharge velocity and density, respectively, and g is gravitational acceleration. The initial jet discharge angle is (ϕ_o, θ_o), where ϕ_o is vertical discharge angle with respect to the horizontal $x-y$ plane, and θ_o is horizontal discharge angle with respect to x-axis. Each individual jet mixes with the ambient current by shear entrainment (close to the source) and vortex entrainment further away, and is bent-over by the current. If the jet momentum is not directed in the (x-z) plane, where z=vertical direction, the jet will have a three-dimensional trajectory. The objective is to predict the unknown plume geometry and the characteristic dilution and velocity in the jet cross section.

The Lagrangian model JETLAG (Lee and Cheung 1990; Lee *et al.* 2000; Lee and Chu 2003) predicts the mixing of buoyant jets with three-dimensional trajectories. In the model, the unknown jet trajectory is viewed as a sequential series of "plume-elements" which increase in mass as a result of shear-induced entrainment (due to the jet discharge) and vortex-entrainment (due to the crossflow) - while rising by buoyant acceleration and being sheared over by the crossflow (Fig. 2). Each plume element, which can be thought of as a section of a bent cone, is characterized by its location, average velocity, pollutant concentration, temperature and salinity, width, and thickness. The model tracks the evolution of the *average* properties of a plume element at each step by conservation of horizontal and vertical momentum, conservation of mass accounting for entrainment, and conservation of tracer mass/heat. The turbulent entrainment of the ambient fluid into the plume element is calculated at each step. Based on the increase in elemental mass, the momentum, energy, and tracer mass conservation equations can be solved in their integral form to give the velocity, density, and concentration at the next step. The kinematic and geometrical relations are then used to give the trajectory and relevant dimensions. Details of the theory and computation can be found in Lee and Cheung (1990) and Lee and Chu (2003).

The early version of JETLAG (Lee and Cheung 1990) was successful with the modelling of many basic flows and unique in its treatment of jets with three-dimensional trajectories. However, the modelling of the transition from the near field (shear entrainment) to the far field (vortex entrainment) has always remained a significant challenge. The shear entrainment hypothesis was based on Schatzmann's hypothesis which lacked a theoretical foundation. Over the past decade, supported by turbulence model computations and detailed laboratory LIF measurements, the entrainment computation has been significantly revised and the general applicability of the model as an impact assessment tool has been greatly enhanced. First, based on a validated theory and experiments of a coflow jet (Chu *et al.* 1999), a general shear entrainment hypothesis is developed (Lee *et al.* 2000). Second, a general method of modelling the transition from the near to the far field has been proposed (Lee *et al.* 2000; Lee and Chu 2003).

The updated version of JETLAG serves as the engine of the PC-based virtual reality software VISJET which was released in 2002 (http://www.aoe-water.hku.hk/visjet).

This technical note is intended as a sequel and accompanying note to the theory described in Lee and Chu (2003). The objective is to document and explain the implementation of the near to far field transition in the code, and to give a comprehensive comparison of model predictions against benchmark experimental data. In this new version of JETLAG (VISJET2008), a general treatment of near-far field transition is implemented in a way that reproduces exactly the asymptotic behavior of advected line thermals and puffs.

2. Entrainment Computation

The crux of the plume model is the computation of turbulent entrainment for the general situation of an arbitrarily-inclined plume element in a crossflow. The increase in mass of the plume element is due to turbulent entrainment of the ambient flow. Close to the discharge point, or in a very weak currrent, shear-induced entrainment dominates. The cross-sectional concentration distribution is radially symmetrical and Gaussian (Fig. 3). In the bent-over phase (the far field), however, the vortex entrainment of the crossflow dominates. The flow is analogous to that of an advected line thermal or puff. The cross-sectional concentration scalar field is horse-shoe shaped, with double concentration peaks. For a buoyant jet in crossflow, the vortex entrainment is typically more significant than the shear entrainment in the far field. In general, however, the relative importance of shear and vortex entrainment varies depending on the flow and the location on the jet trajectory.

The increase in mass of the plume element at each step, ΔM, is computed as a function of two components: the shear entrainment due to the relative velocity between the plume element and the ambient velocity in the direction of the jet axis, ΔM_s, and the vortex entrainment ("forced" entrainment) due to the ambient crossflow, ΔM_f. Details on the computation of ΔM_s and ΔM_f can be found in Lee and Chu (2003).

The total entrainment

The total entrainment can be obtained from a maximum hypothesis, $\Delta M = Max(\Delta M_s, \Delta M_f)$; alternatively an additive hypothesis, $\Delta M = \Delta M_s + \Delta M_f$ can be used. Comparison with basic data shows that the maximum hypothesis in general gives better results. In the far field, when the buoyant jet is significantly bent over, it is well known that the flow behavior asymptotically approaches that of an advected line thermal. This asymptotic behavior would be faithfully reproduced by the maximum hypothesis (as adopted in the earlier version of the model, JETLAG98). However, the use of this hypothesis may give unreasonable predictions for a weak current. When U_a is small, e.g. around tidal slack, or when Q_o is large, or during the initial phase of a counterflow, it is expected that shear entrainment dominates. However, the relative jet velocity decreases as the ambient current increases - thus leading to a decrease in entrainment with increasing crossflow, a result that is not borne out by experiments of plumes in weak crossflow (Lee and Cheung 1991). Neither of these two approaches can reproduce satisfactorily the initial mixing data in the near to far field (bdnf-bdff) transition (Lee and Cheung 1991). A general model is needed to handle the transition from the shear entrainment (advected jet/plume) regime to the vortex entrainment (advected puff/thermal) regime.

Consider the general situation of a jet/plume in a crossflow, with the jet axis making an angle of ψ_k with the crossflow (Fig. 4); the ambient current in the plane of the jet cross-section is then $U_a \sin\psi_k$. A heuristic general

entrainment formulation, which models the near-far field transition (or weak to strong current), can be written as:

$$\Delta M = E_s \frac{(\pi - \varphi_k)}{\pi} + E_f \ \sin\varphi_k \tag{1}$$

where φ_k is a "separation angle" which delineates the relative importance of shear and vortex entrainment, and E_s, E_f = shear and vortex entrainment respectively. φ_k is computed from the maximum radial shear entrainment velocity and the ambient velocity according to:

$$\cos(\varphi_k) = Min(\frac{V_r(max)}{U_a \sin\psi_k}, 1) \tag{2}$$

For a round jet or plume in stagnant fluid, the longitudinal jet velocity is self-similar and approximately Gaussian; the radial entrainment velocity field V_r can be obtained from continuity as a function of the local centerline velocity. At each step, the separation angle, φ_k, and the entrainment terms E_s and E_f can be locally determined. Details can be found in Lee and Chu (2003).

Eq.2 and Eq.1 show that as $U_a \to 0$, $\varphi_k \to 0$, $\Delta M \to E_s$; i.e. the entrainment is entirely due to shear entrainment, while as $U_a \to \infty$, $\varphi \to \pi/2$ - i.e. entrainment is almost entirely due to crossflow (E_f typically much greater than E_s). In the limiting case of an advected line thermal, with $\varphi = \pi/2$, Eq. 1 gives a result that is slightly larger than the desired limit of $\Delta M \approx E_f$, with $\Delta M = \frac{E_s}{2} + E_f$. Extensive model testing against benchmark laboratory data suggests that model performance can be optimized with a modified implementation of Eq.1:

$$\Delta M = E_s \frac{(\pi - \varphi_k)}{\pi}(1 - \sin^n \varphi_k) \ + \ E_f \ \sin\varphi_k \tag{3}$$

where $f(\varphi_k) = (1 - \sin^n \varphi_k)$ ensures that the turbulent entrainment is due to only vortex entrainment as $\varphi \to \pi/2$ in the far field. Tests showed that $n = 100$ gives good results.

Alternatively, $f(\varphi_k) = \tanh(A(\pi/2 - \varphi_k))$, with $A = 6 - 10$ would give similar results.

$$\Delta M = E_s \frac{(\pi - \varphi_k)}{\pi} \tanh(6(\pi/2 - \varphi_k)) \ + \ E_f \ \sin\varphi_k \tag{4}$$

The nature of this near-far field transition can be best illustrated by three examples. Fig.5 shows the predicted trajectory of a horizontal buoyant jet in a coflowing current for jet densimetric Froude number $Fr = 15$ and jet to ambient current ratio $K = 5$. It can be seen that the observed trajectory is well-predicted (top figure; solid line: theory; symbols:data). The bottom figure shows the variation of the separation angle, shear and vortex entrainment with x/D. Initially the jet is dominated by shear entrainment, with $f(\varphi_k) = 1$. As the jet rises by buoyancy, the separation angle increases gradually from zero to $\pi/2$. It is seen that the entrainment is dominated by the vortex entrainment. Fig.6 shows a similar example for a vertical buoyant jet in crossflow (experiments of Fan). It is seen that the separation angle increases gradually from zero to $\pi/2$ as the jet becomes bent over; the relative small proportion of shear entrainment explains why even models that treat only the far field (Chu 1975) can predict the trajectory so well. Fig.7 shows a counterflow buoyant jet in a stratified crossflow; the jet discharges against the current, and is bent over after rising a certain distance. It is seen that both the shear and vortex entrainment are not negligible, and that using Eq. 3 the total entrainment evolves from shear entrainment smoothly to the correct limiting case. On the contrary, the use of an additive hypothesis may give rise to excessive entrainment that is not physically realistic.

3. COMPARISON OF MODEL PREDICTIONS WITH EXPERIMENTAL DATA

The ultimate test of the heuristic model is validation against experimental data. The model predictions are compared with extensive benchmark test data for a wide range of flows. The predicted trajectory (in both the momentum and buoyancy planes) and centerline tracer concentration are compared with observations for the following cases (Fig.8 to Fig.20):

- Vertical buoyant jet in crossflow (Fan 1967) for different nominal values of jet densimetric Froude number F and jet to ambient velocity ratio $K = U_j/U_a$
- Horizontal buoyant jet in coflowing current (Ayoub 1971)
- Horizontal buoyant jet in coflowing current (Knudsen 1989); this set of data extends the range of the trajectory, as well as F and K, beyond the experiments of Ayoub.
- Horizontal buoyant jet in crossflow, with a 3D jet trajectory (Ayoub 1971); comparisons are shown both for the momentum (x-y) and buoyancy (x-z) planes.
- Horizontal buoyant jet in crossflow, with a 3D trajectory (Chu 1975); covers more buoyant discharges (low F) with stronger currents.
- Horizontal heated jet in crossflow, with a 3D trajectoy (Cheung 1990); buoyant plumes (small F) in a crossflow. In this set of experiments the scalar field in the jet cross-section is also measured, thus enabling the determination of the average concentration. For this set of experiments, the predicted and measured average concentration are compared.
- Oblique jet in crossflow (Chu 1985); momentum jets discharged at various angles to the crossflow.
- Dense plume in crossflow (Chu 1975)
- Vertical buoyant jet in stratified crossflow (Wright 1979); prediction of maximum and equilibrium height of rise
- Buoyant plume in weak crossflow (Lee and Cheung 1991); note the pick up of dilution in a weak crossflow, for $z/l_b \approx 0.1 - 1$.
- Buoyant jet in counterflow (Lam *et al.* 2006)

4. CONCLUSIONS

In general, it can be seen the model predictions of jet trajectory and tracer concentration compare remarkably well with the benchmark data for a wide range of flow scenarios. Extensive tests (not shown) also demonstrate that the use of the hyperbolic tangent transition factor with $A = 6$ gives graphically indistinguishable predictions as the use of Eq.3 with $n = 100$. In particular, the practically important case of a buoyant jet in stratified crossflow and a jet in counterflow - two complex flow that are very difficult to model - are reasonably well predicted. The observed significant increase in dilution in a weak crossflow in the near-far field transition is also well-predicted. In the

few cases where less than satisfactory model-data agreement is noted, the discrepancy may be attributed to possible experimental inconsistency or difficulties (e.g. the horizontal buoyant jet in crossflow experiments of Ayoub, F=15, K=15), or difficult areas where further research and additional data are required (e.g. dense plumes or counter-flow jets in crossflow).

For the majority of cases, the predictions of both the present model (JETLAG2008) and the earlier version (JETLAG99 as embodied in VISJET2002) give similarly good results. This is expected as Eq.3 or Eq.4 is a practically equivalent but more robust version of the *ad hoc* treatment of the transition modelling in JETLAG99. Eq.3 (or Eq.4) gives correctly a smooth transition from the shear entrainment (E_s) in the near field to the vortex entrainment (E_f) in the far field. In addition, the model has also been tested to work well for the entire range of ambient and discharge conditions of the Hong Kong Harbour Area Treatment Scheme (Choi *et al.* 2008, submitted).

Besides providing a theoretical basis for predicting the mixing in the transition from the near to far field (one is often concerned with the transition regime in practical problems), the advantages of the transition modelling can be illustrated by a few examples. In Fig. 16 the predictions of the maximum and equilibrium height of rise of a vertical buoyant jet in stratified crossflow (a practically important case) are compared with the data of Wright (1979). It can be seen that the present model (with transition modelling) gives significantly more accurate predictions than those of JETLAG98 (which uses a maximum hypothesis). Similarly, Fig.21 shows the model predictions of a horizontal buoyant jet in coflow against the data of Knudsen. It can be seen the maximum hypothesis (JETLAG98) significantly overpredicts the rise of the jet trajectory, except for the case of $K = 1$. For this case, the jet velocity is equal to the ambient velocity, $u_a = u_j$, and we have an exact advected line thermal, with $E = E_f$; hence the maximum hypothesis would be practically the same as the transition model. Finally, the difficulty of using a maximum entrainment hypothesis is illustrated with a practical example. In Fig. 22 the variation of predicted surface dilution is shown as a function of ambient current for the buoyant plume of the Sydney deepwater outfall (port discharge $Q_o = 0.264\ m^3/s$, port diameter $D = 0.3$ m, discharge and ambient salinity and temperature: $S_o = 0$ psu, $T_o = 25^oC$, $S_a = 35$ psu, $T_a = 17^oC$). For small ambient current speeds, the predicted buoyant plume trajectory (bottom figure) is near vertical by virtue of the large buoyant discharge (large buoyancy flux). As the current increases, however, the predicted dilution by the maximum entrainment hypothesis actually *decreases* in the range of u_a =0.05-0.1 m/s - a physically unreasonable result that is not supported by experiments. The relative role of shear and vortex entrainment is illustrated in Fig.23 for three representative current speeds - $u_a = 0.01, 0.08, 0.3$ m/s. It can be seen that for a weak current, $u_a = 0.01$ m/s, the dilution is solely due to shear entrainment over the entire depth. As the current increases, the relative importance of E_s and E_f depends on the location; as the plume rises (e.g. $u_a = 0.08$ m/s, middle figure) the entrainment is increasingly dominated by the vortex entrainment.

Acknowledgements

David Choi, Ken Lee and Adrian Lai assisted with the testing of the model.

References

[1] Chu, P.C.K. (1996). “Mixing of turbulent advected line puffs,” PhD thesis, The University of Hong Kong, Hong Kong.

[2] Chu, P.C.K., Lee, J.H.W. and Chu, V.H. (1999). “Spreading of turbulent round jet in coflow,” *Journal of Hydraulic Engineering*, ASCE, 125(2), pp. 193-204.

[3] Lam, K.M., Lee, W.Y., Chan, C.H.C. and Lee, J.H.W. (2006). ”Global behavior of a round buoyant jet in a counterflow”, *Journal of Hydraulic Engineering*, ASCE, 132(6), pp.589-604.

[4] Lai, A.C.H., Yu, D.Y., and Lee, J.H.W. (2008). ”Mixing of a rosette jet group in a crossflow”, *Journal of Hydraulic Engineering*, ASCE (in preparation)

[5] Lee, J.H.W. and Cheung, V. (1990). “Generalized Lagrangian model for buoyant jets in current,” *Journal of Environmental Engineering*, ASCE, 116(6), pp. 1085-1105.

[6] Lee, J. H. W. and Cheung, V. (1991) “Mixing of buoyancy-dominated jets in a weak current,” *Proc. Inst. of Civil Engineers*, 91(2), pp. 113-129.

[7] Lee, J.H.W., Cheung, V., Wang, W.P. and Cheung, S.K.B. (2000). ” Lagrangian modeling and visualization of rosette outfall plumes”, Proceedings of the Hydroinformatics 2000, University of Iowa, Jul. 2000.

[8] Lee, J.W.W. and Chu, V.H. (2003). *Turbulent Jets and Plumes - a Lagrangian Approach*. Kluwer Academic Publishers, Boston.

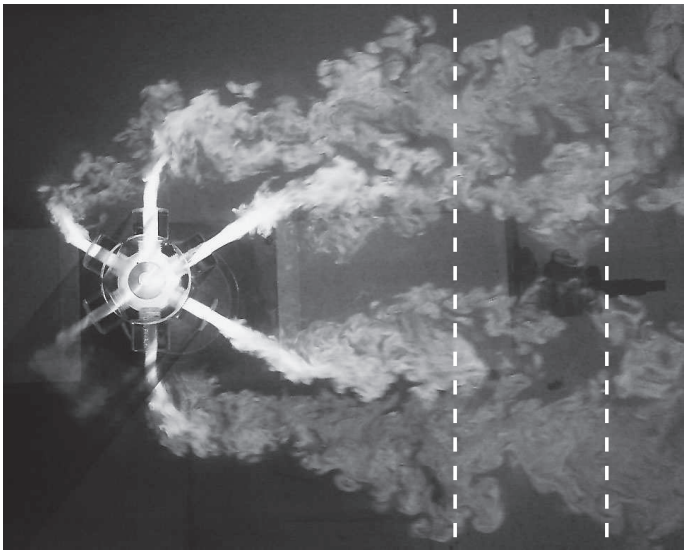

Fig. 1: A 6-jet rosette jet group in crossflow (current from left to right)

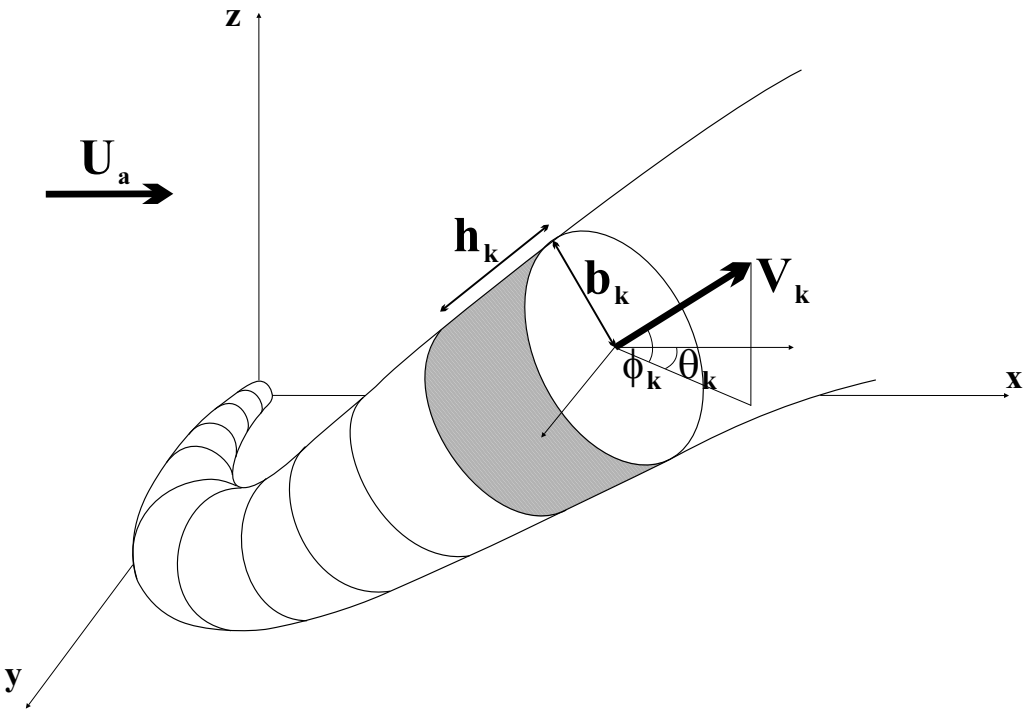

Fig. 2: General Lagrangian model for buoyant jet with three-dimensional trajectories; schematic diagram of jet trajectory traced out by Lagrangian plume elements

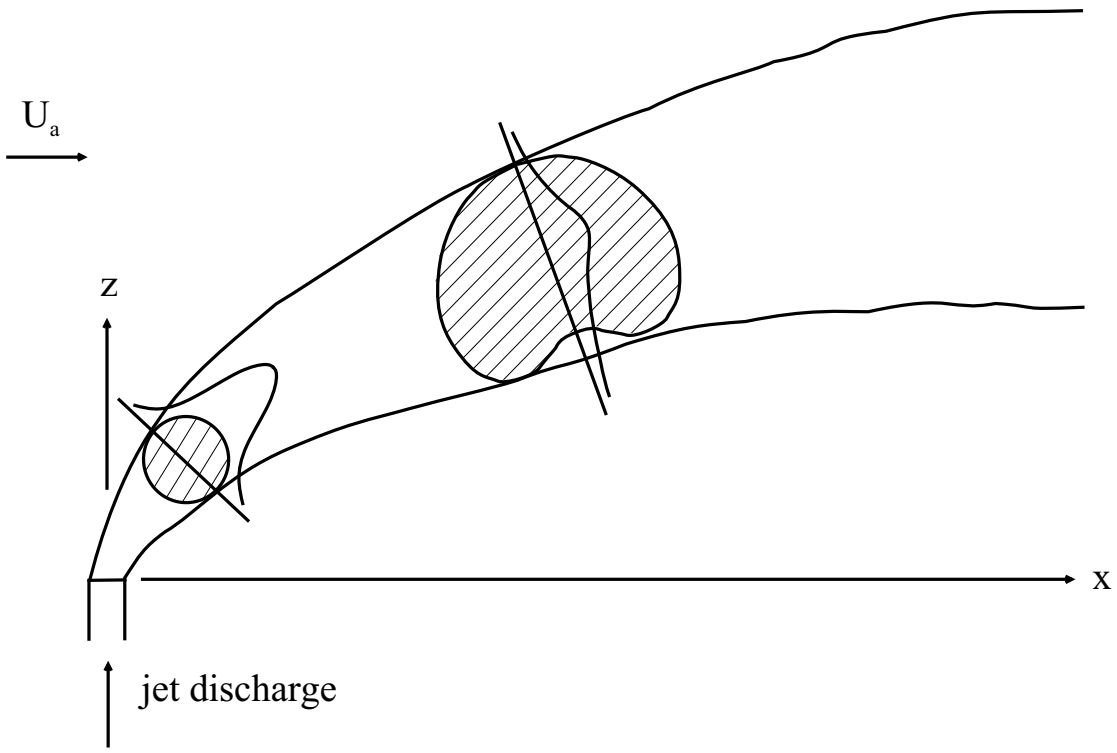

Fig. 3: Asymptotic flow regimes showing the transition from a Gaussian concentration profile in the near field to the vortex-pair profile in the far field

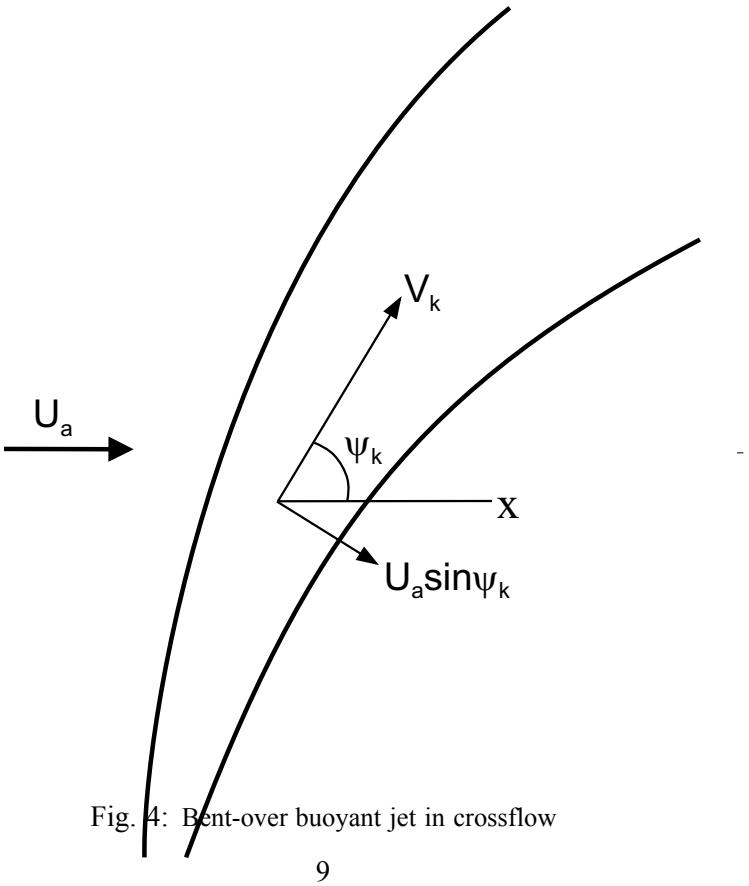

Fig. 4: Bent-over buoyant jet in crossflow

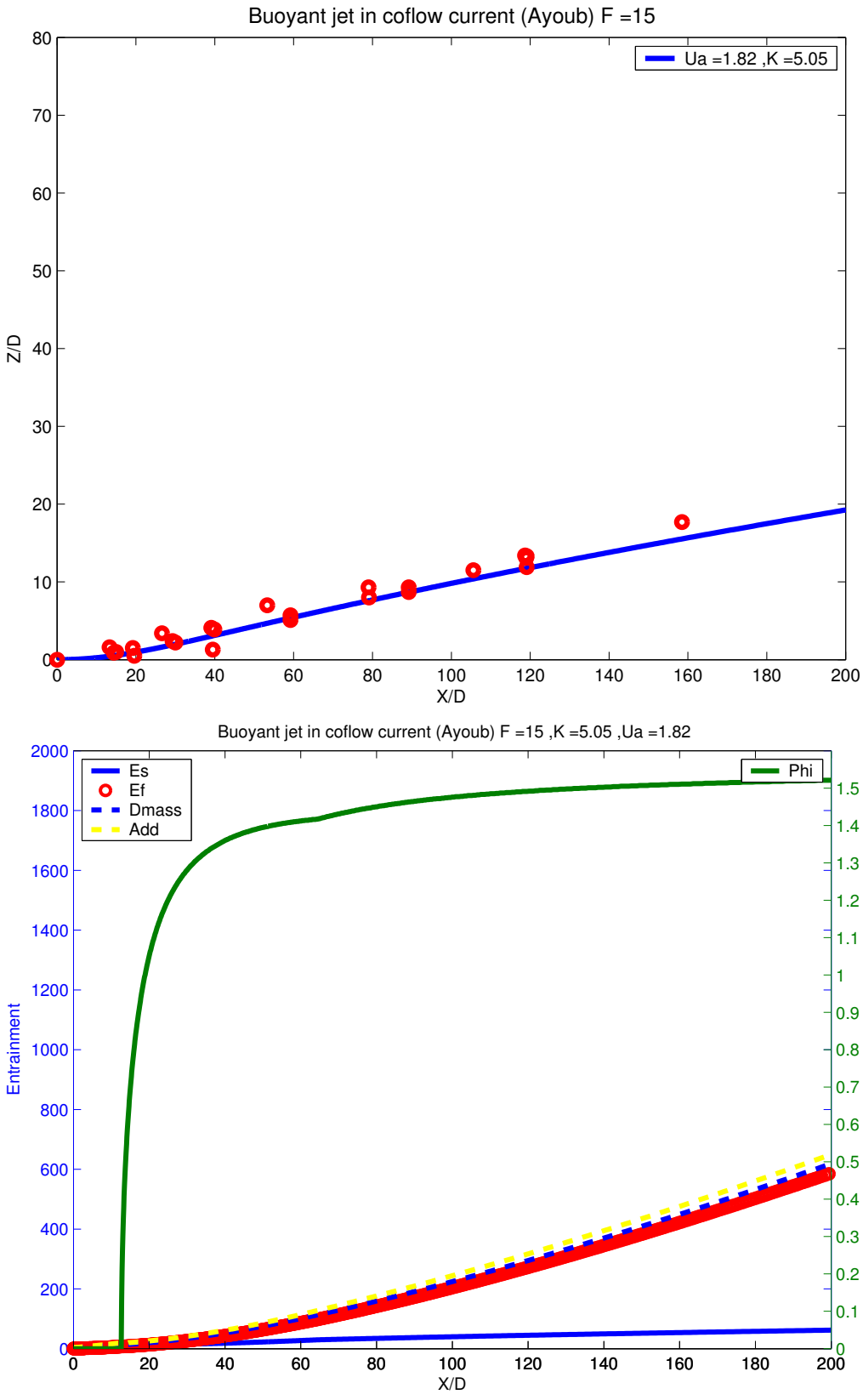

Fig. 5: Horizontal buoyant jet in coflow: (top) predicted trajectory and data (symbols); (bottom) variation of separation angle, shear entrainment (E_s), vortex entrainment (E_f) and total entrainment (DMass) along the jet trajectory; additive hypothesis also shown.

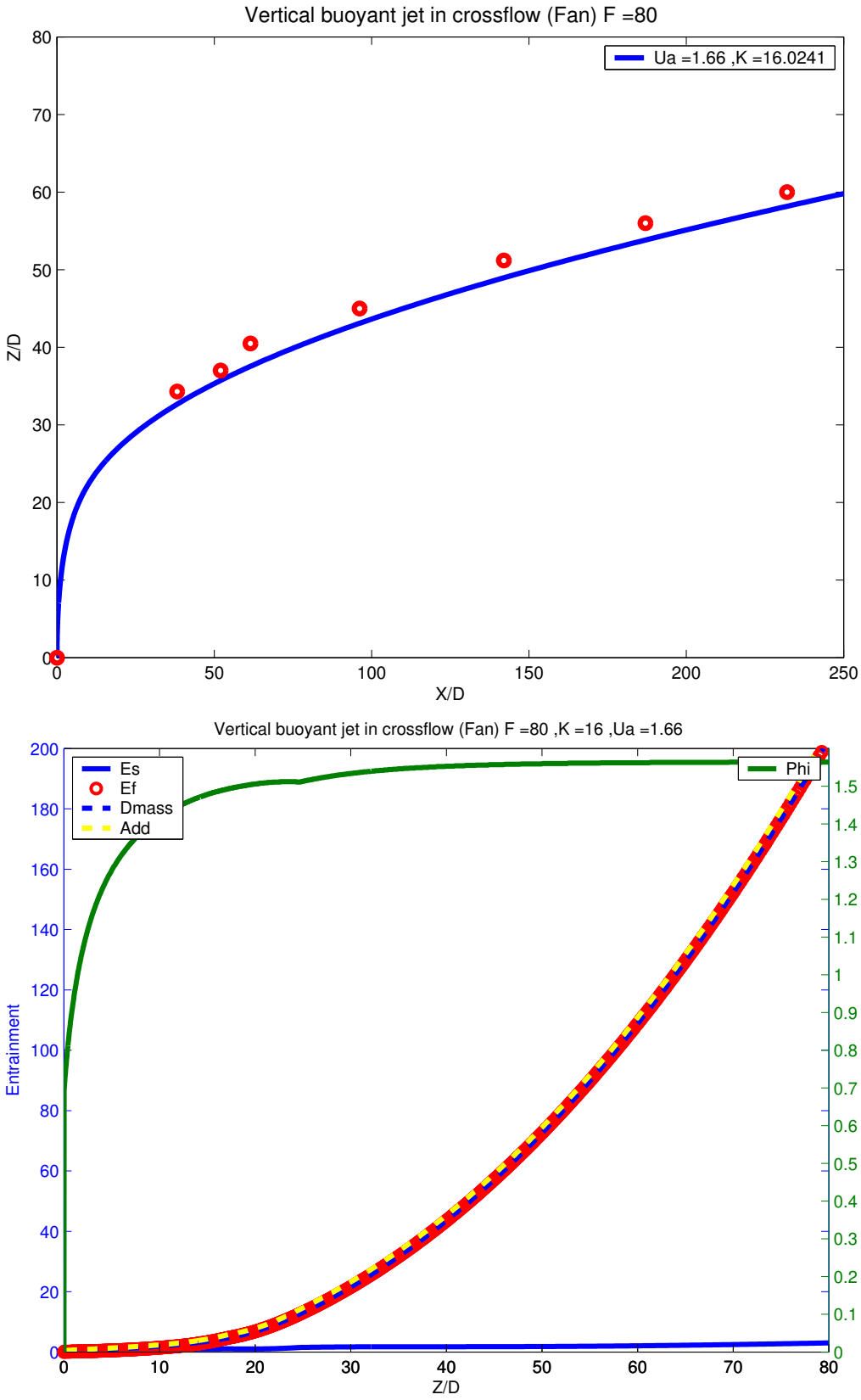

Fig. 6: Vertical buoyant jet in crossflow: (top) predicted trajectory and data (symbols); (bottom) variation of separation angle, shear entrainment (E_s), vortex entrainment (E_f) and total entrainment (DMass) along the jet trajectory; additive hypothesis also shown.

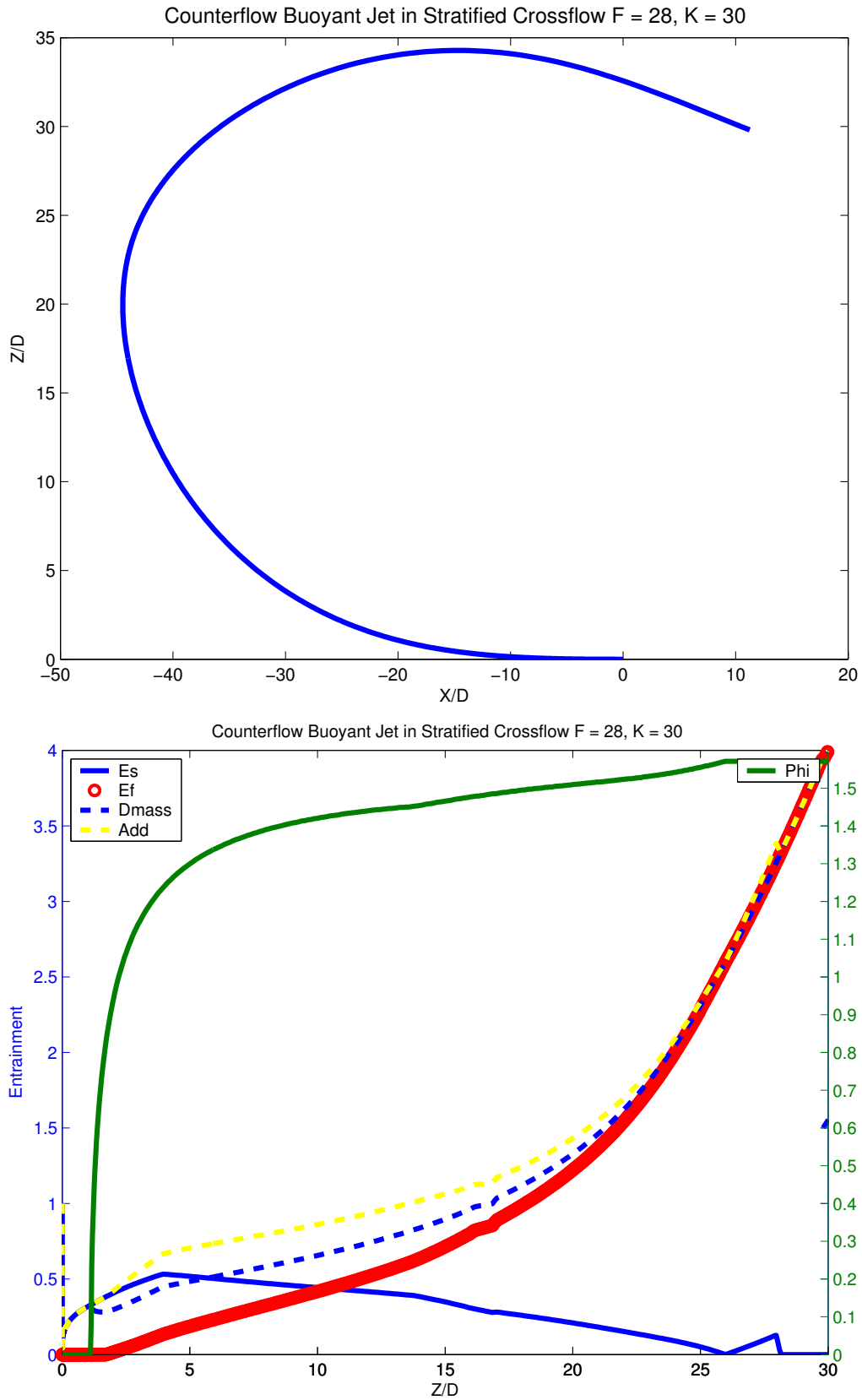

Fig. 7: Counterflow buoyant jet in stratified crossflow: (top) predicted trajectory; (bottom) variation of separation angle, shear entrainment (E_s), vortex entrainment (E_f) and total entrainment (DMass) along the jet trajectory; additive hypothesis also shown.

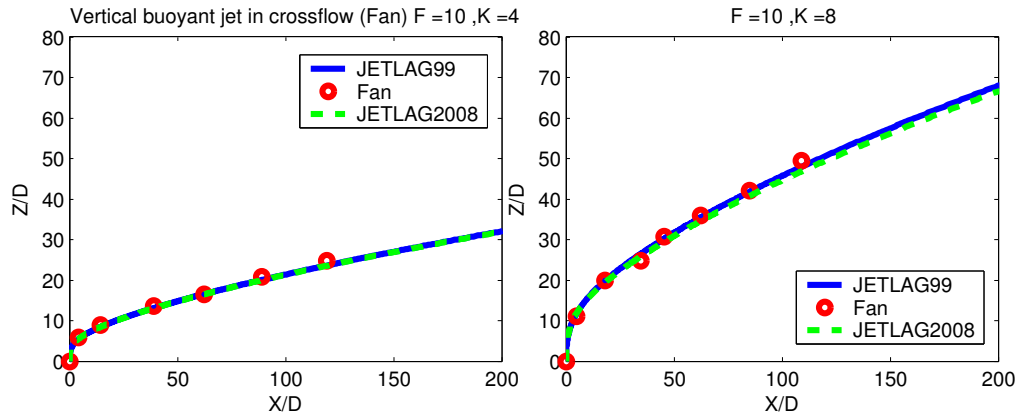
Vertical buoyant jet in crossflow (Fan) F =10 ,K =4
F =10 ,K =8
JETLAG99
Fan
JETLAG2008
Z/D
X/D

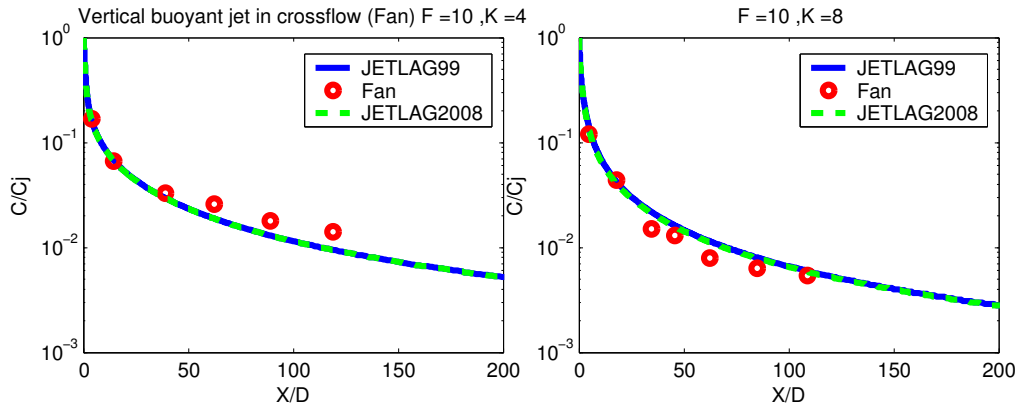
Vertical buoyant jet in crossflow (Fan) F =10 ,K =4
F =10 ,K =8
JETLAG99
Fan
JETLAG2008
C/Cj
X/D

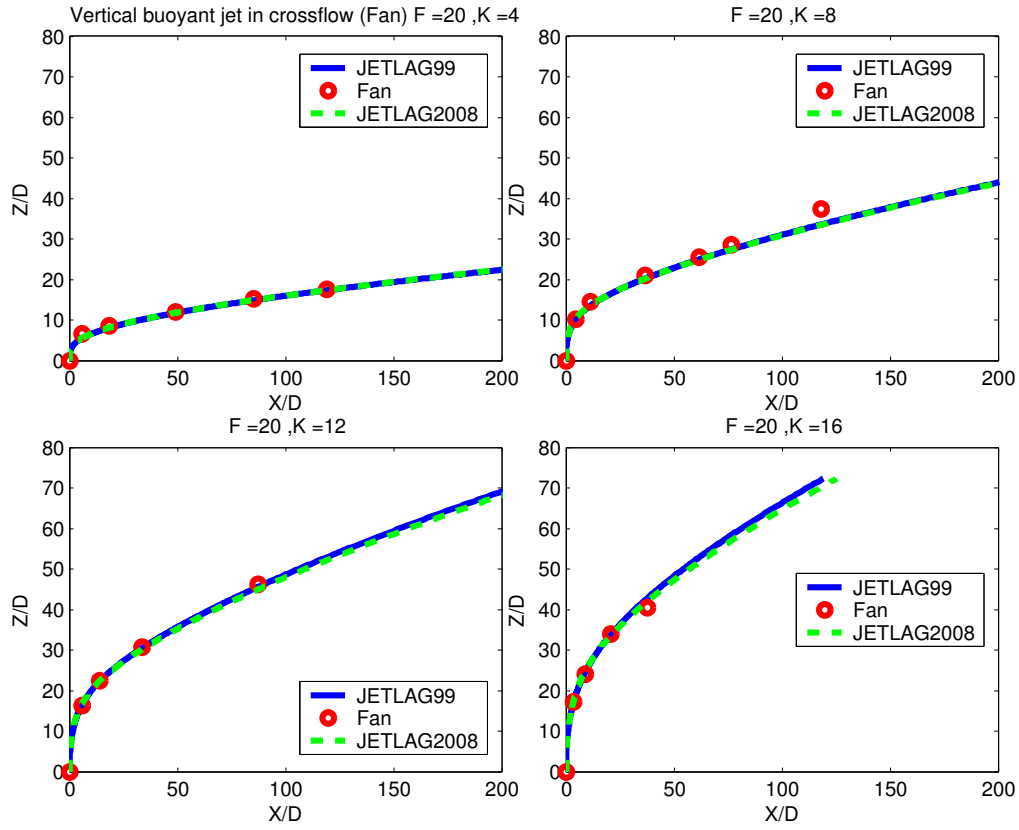
Vertical buoyant jet in crossflow (Fan) F =20 ,K =4
F =20 ,K =8
F =20 ,K =12
F =20 ,K =16
JETLAG99
Fan
JETLAG2008
Z/D
X/D

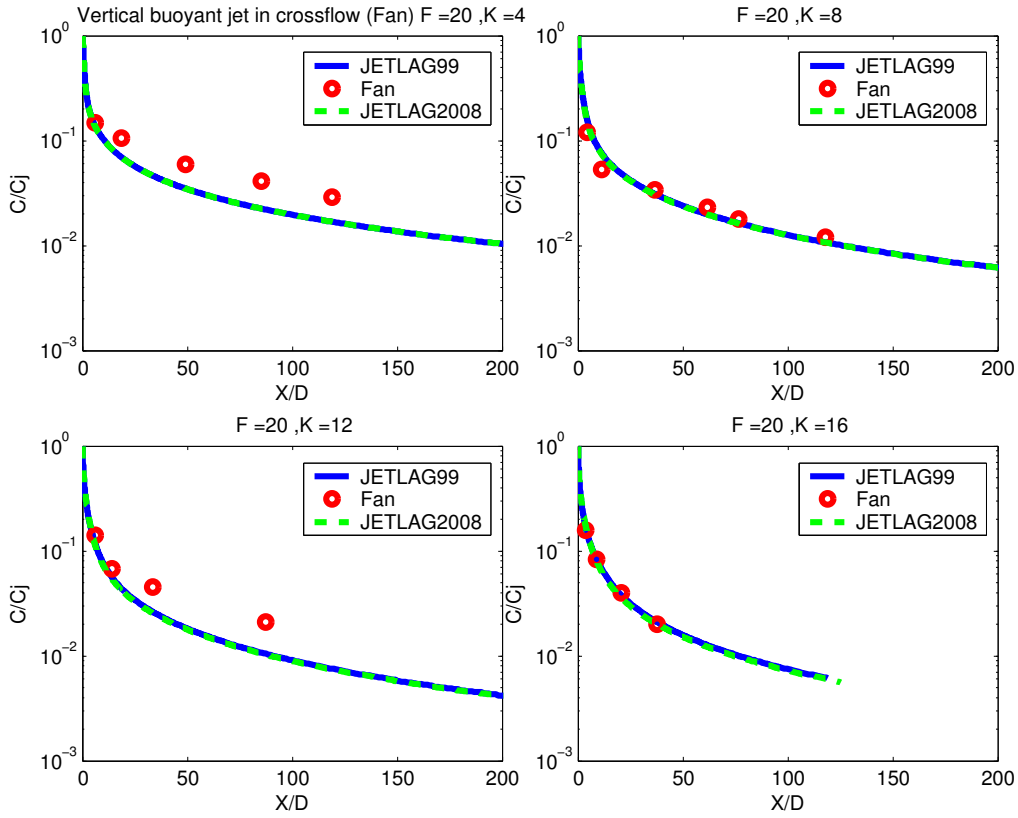
Vertical buoyant jet in crossflow (Fan) F =20 ,K =4
F =20 ,K =8
F =20 ,K =12
F =20 ,K =16
JETLAG99
Fan
JETLAG2008
C/Cj
X/D

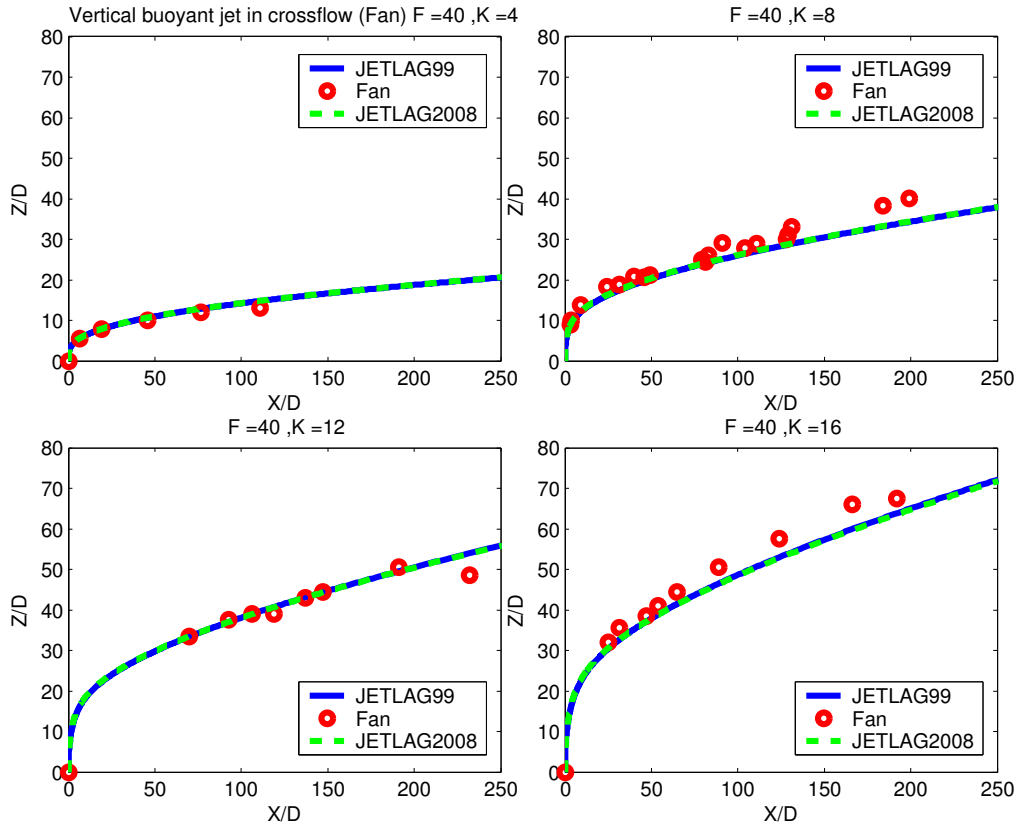
Vertical buoyant jet in crossflow (Fan) F =40 ,K =4
F =40 ,K =8
F =40 ,K =12
F =40 ,K =16
JETLAG99
Fan
JETLAG2008
Z/D
X/D

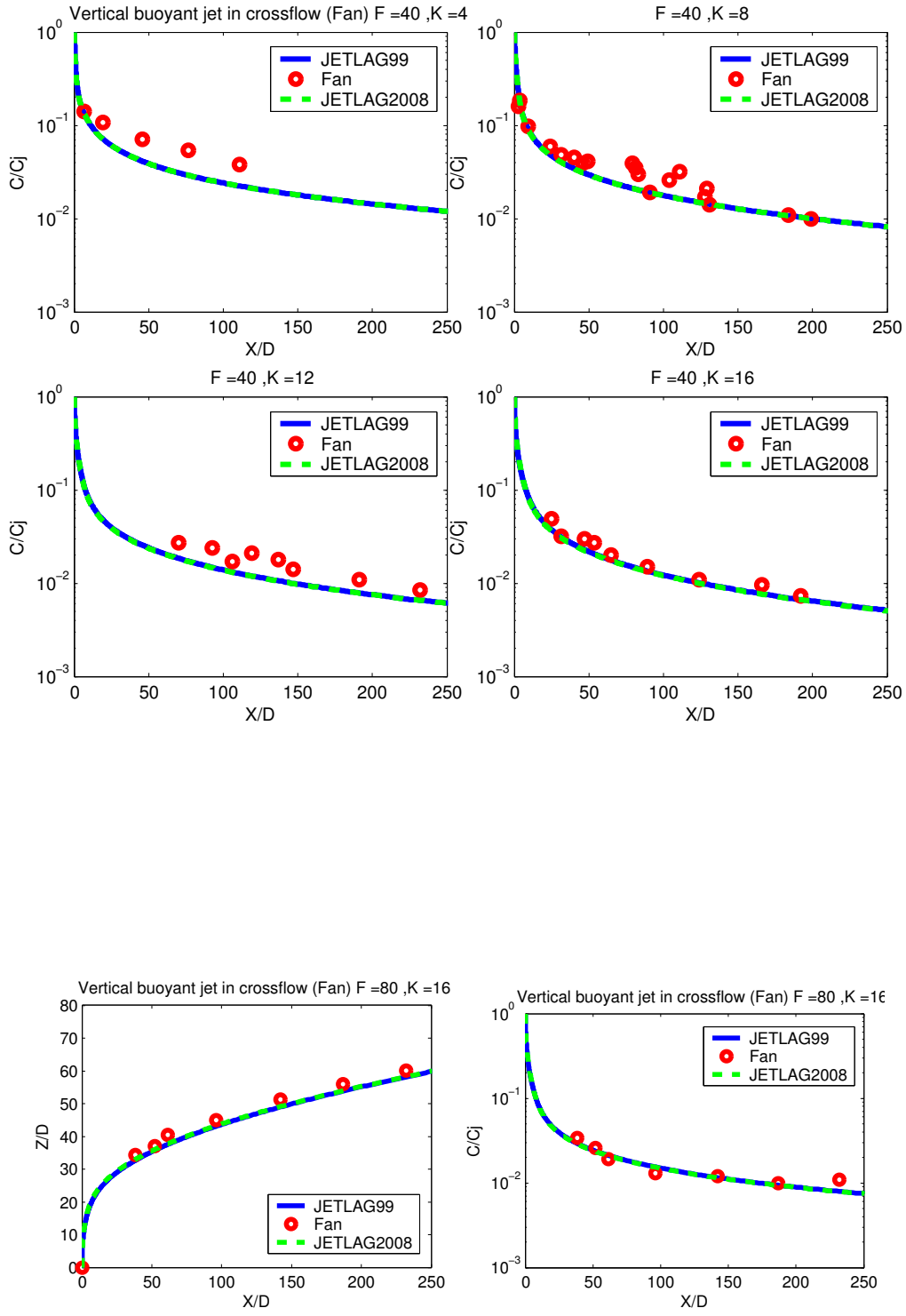

Fig. 8: Comparison of model prediction with data: vertical buoyant jet in crossflow (Fan)

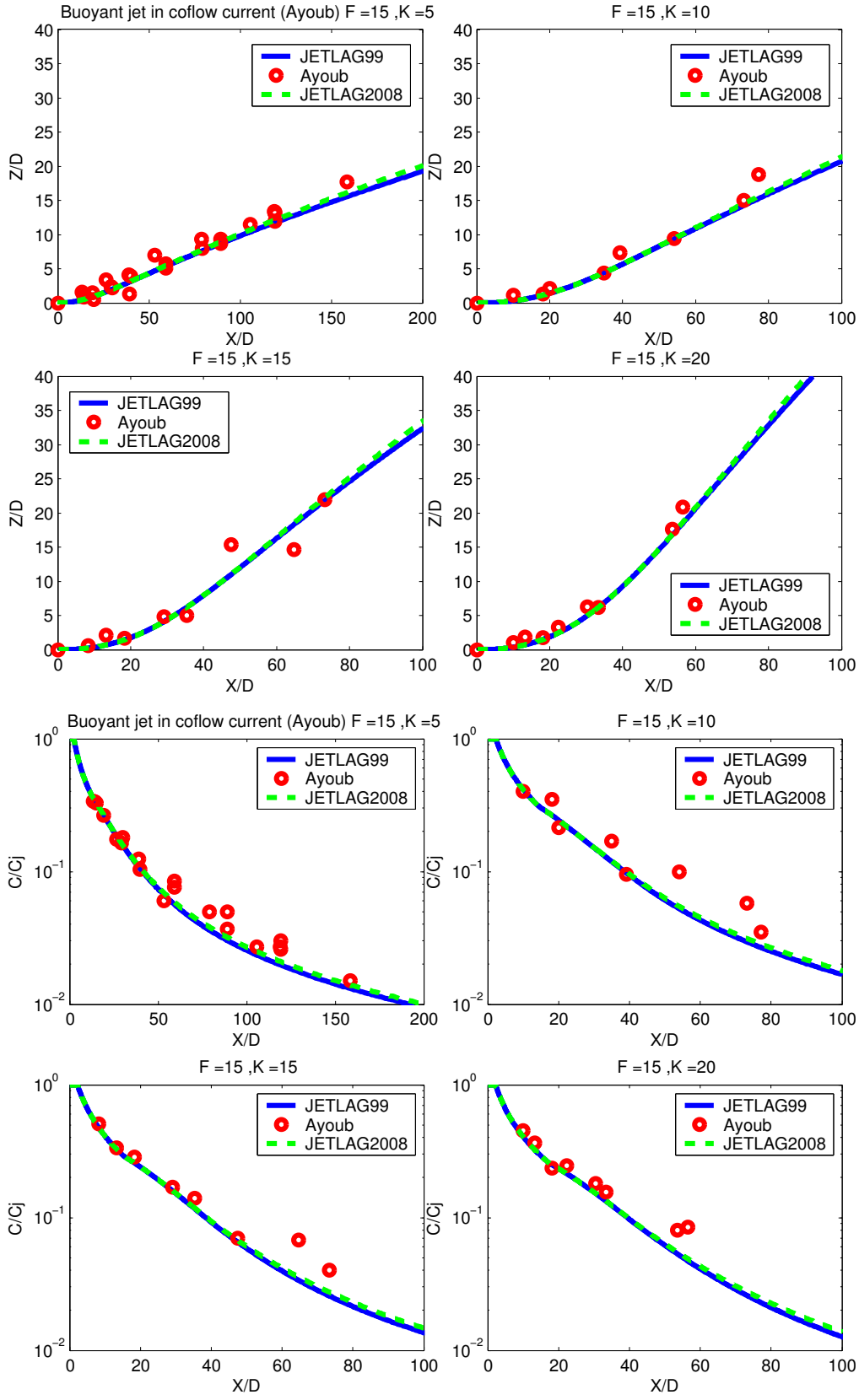
Buoyant jet in coflow current (Ayoub) F =15 ,K =5
F =15 ,K =10
F =15 ,K =15
F =15 ,K =20
JETLAG99
Ayoub
JETLAG2008
Z/D
X/D
C/Cj

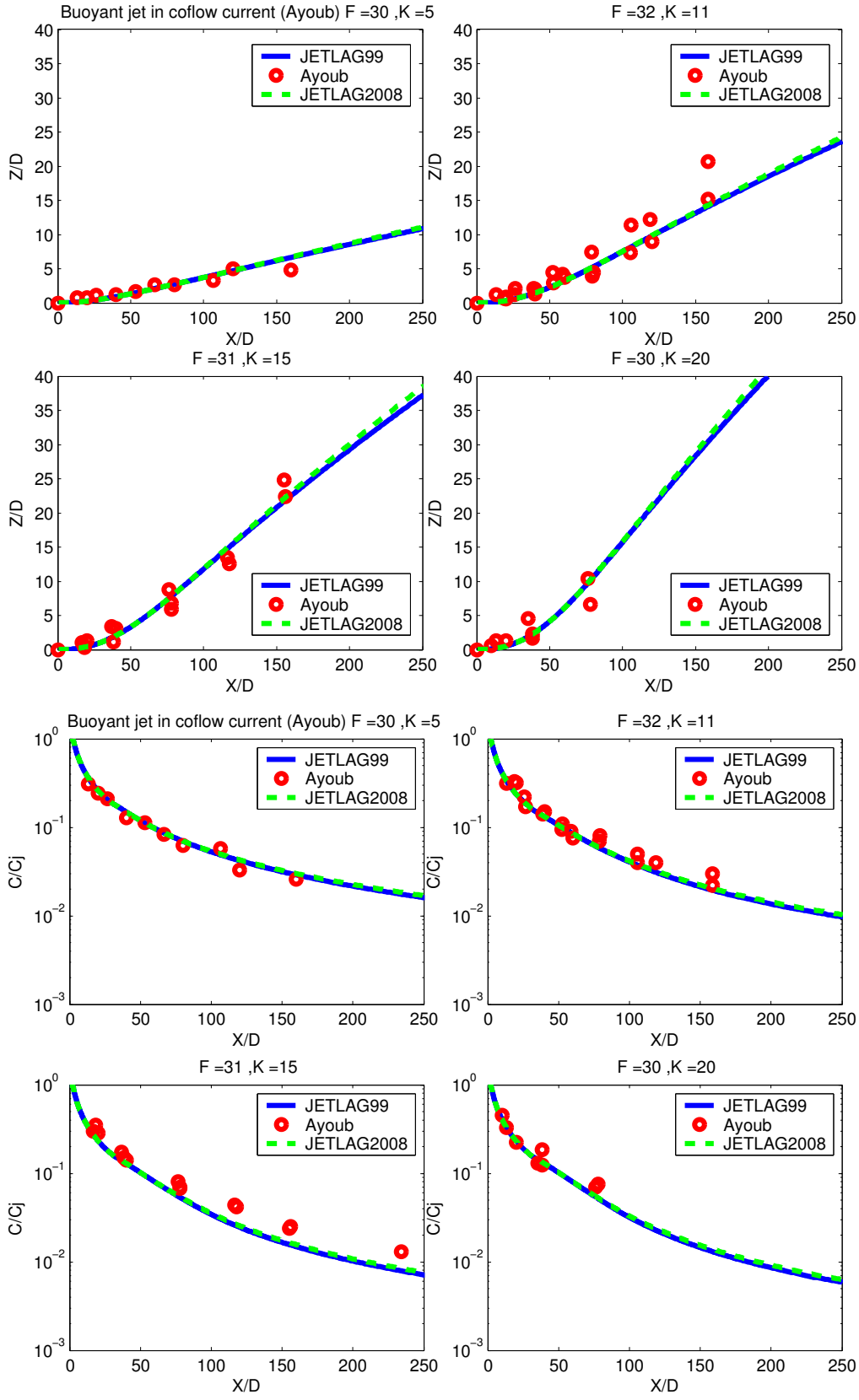
Buoyant jet in coflow current (Ayoub) F =30 ,K =5
F =32 ,K =11
F =31 ,K =15
F =30 ,K =20
JETLAG99
Ayoub
JETLAG2008
Z/D
C/Cj
X/D

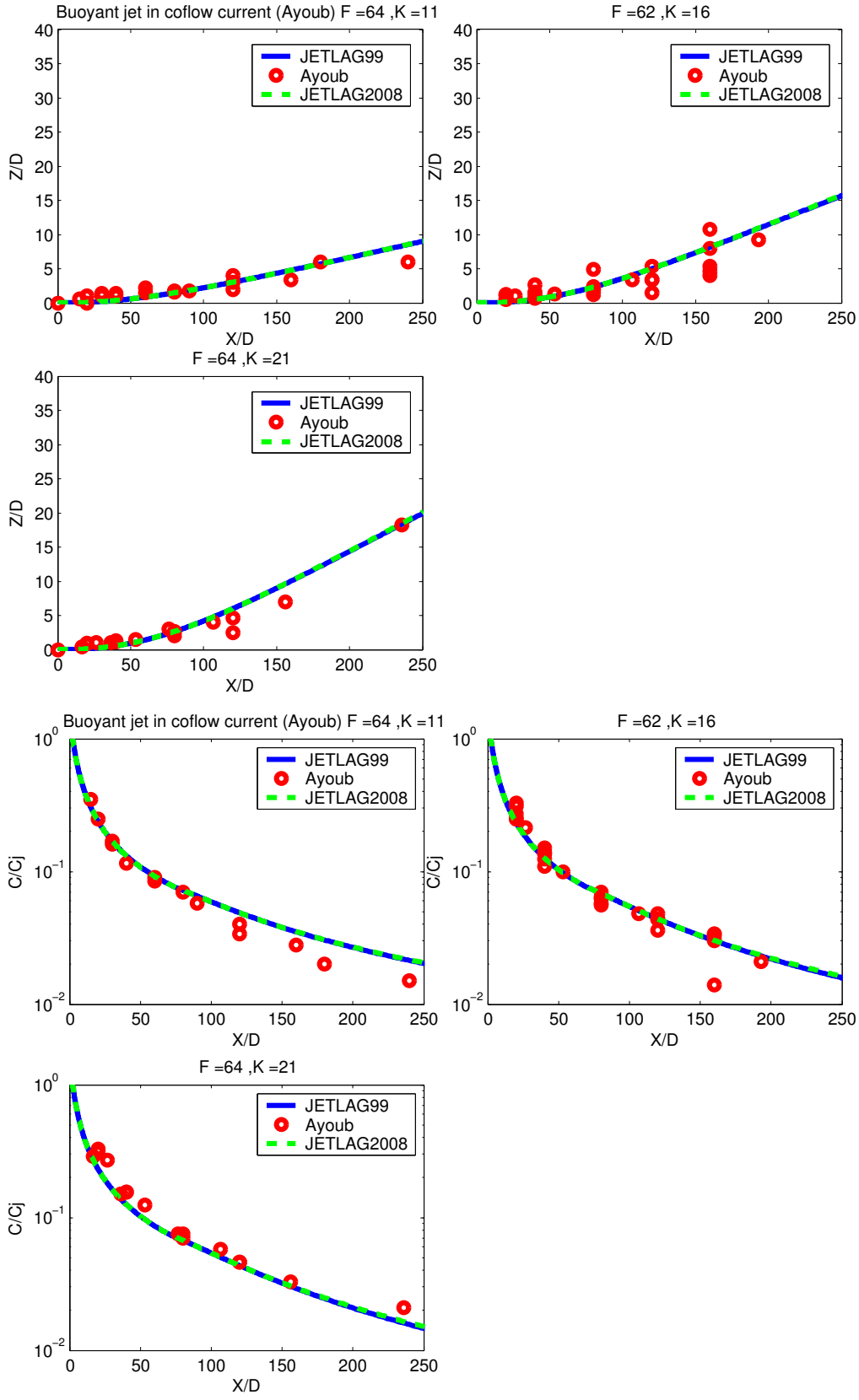
Buoyant jet in coflow current (Ayoub) F =64 ,K =11
F =62 ,K =16
F =64 ,K =21
Buoyant jet in coflow current (Ayoub) F =64 ,K =11
F =62 ,K =16
F =64 ,K =21
JETLAG99
Ayoub
JETLAG2008
Z/D
C/Cj
X/D

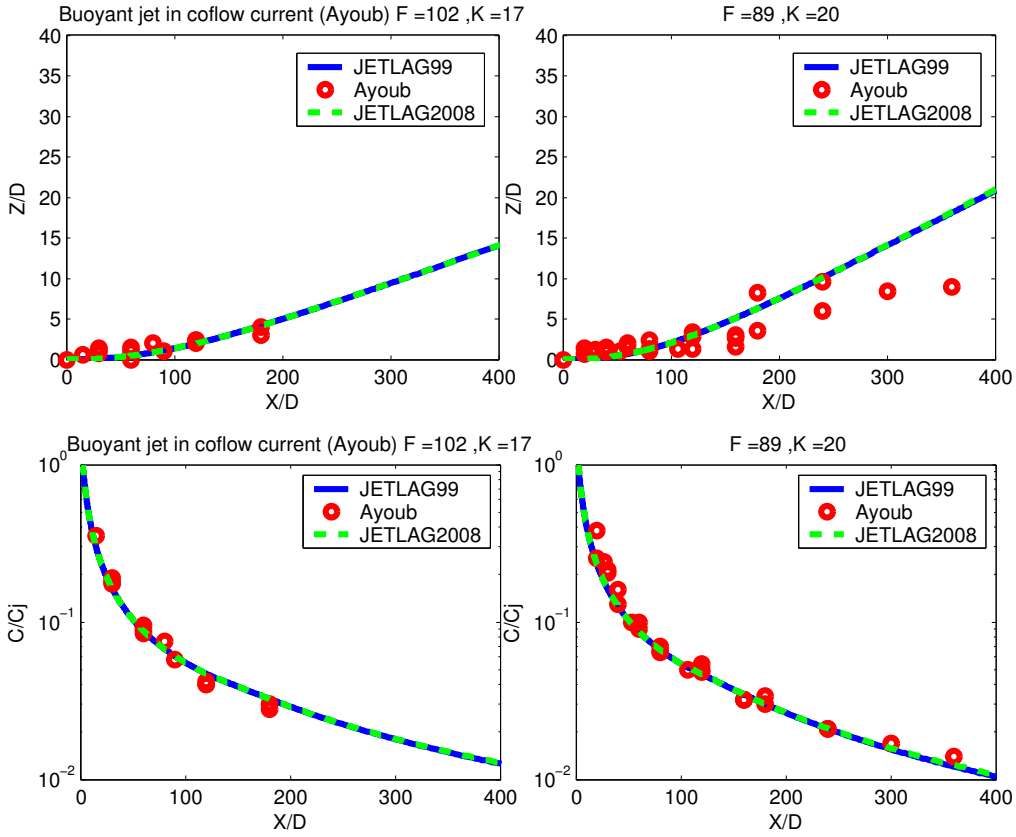

Fig. 9: Comparison of model prediction with data: horizontal buoyant jet in coflowing current (Ayoub)

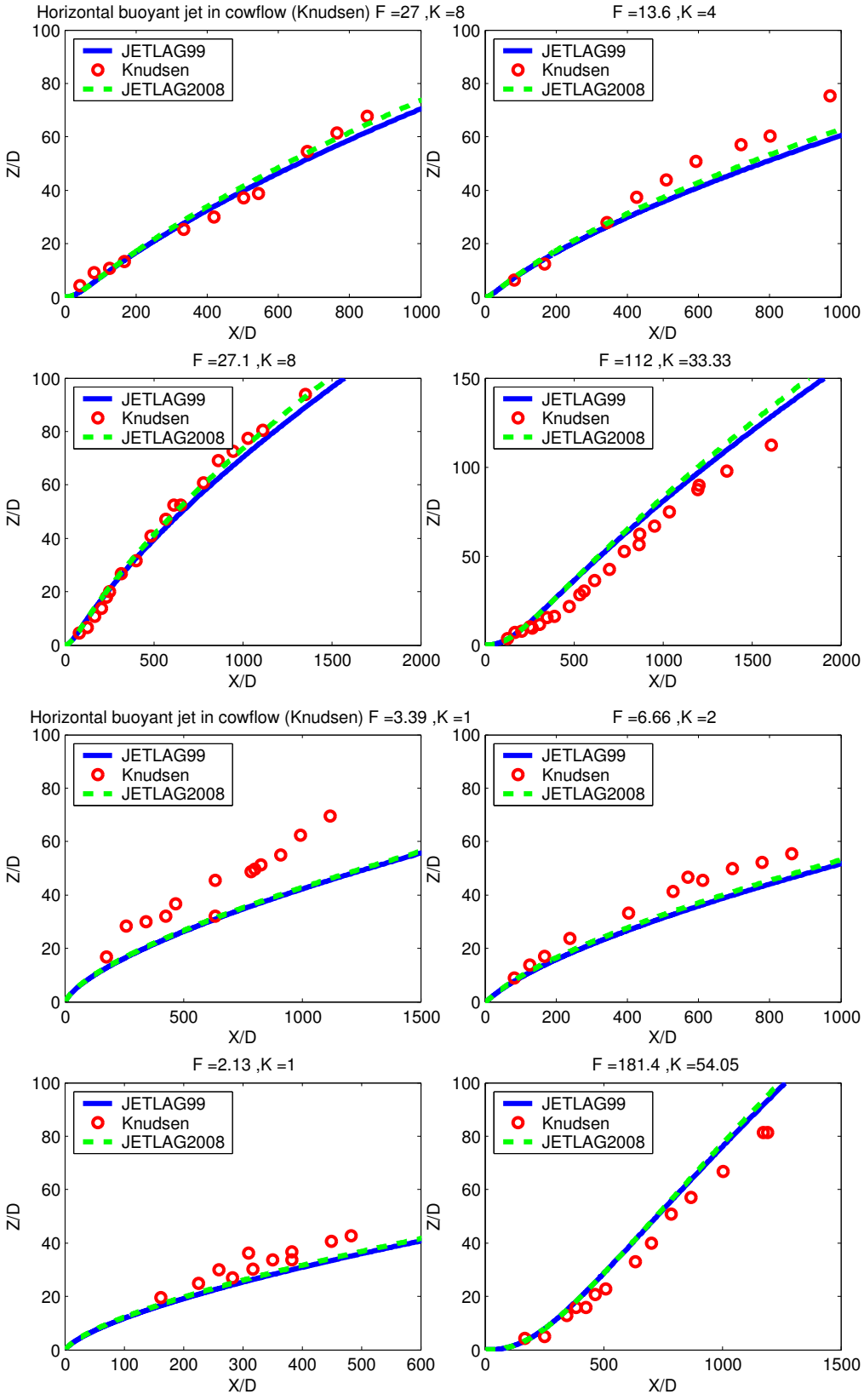
Horizontal buoyant jet in cowflow (Knudsen) F =27 ,K =8
F =13.6 ,K =4
F =27.1 ,K =8
F =112 ,K =33.33
Horizontal buoyant jet in cowflow (Knudsen) F =3.39 ,K =1
F =6.66 ,K =2
F =2.13 ,K =1
F =181.4 ,K =54.05
JETLAG99
Knudsen
JETLAG2008
Z/D
X/D

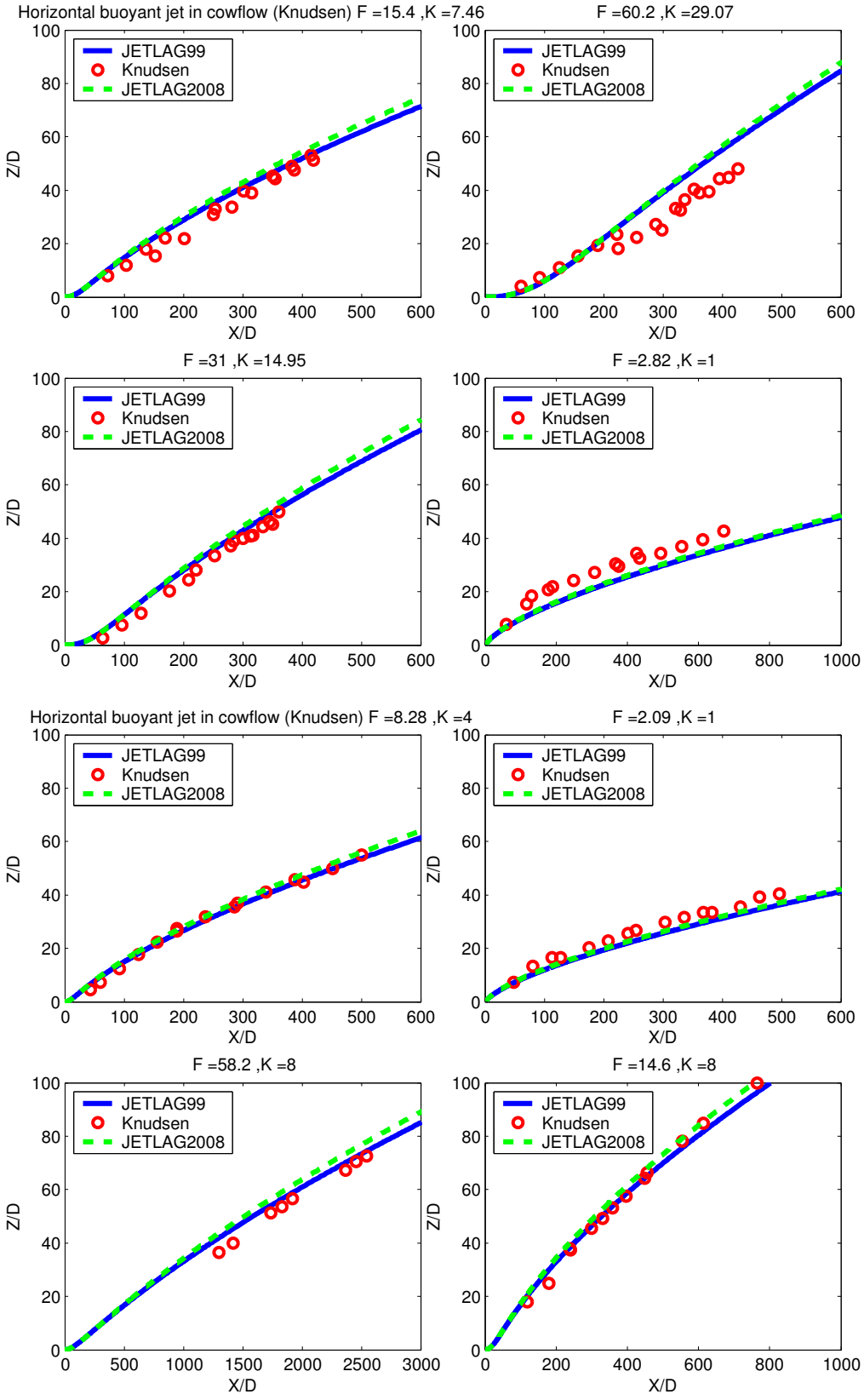
Horizontal buoyant jet in cowflow (Knudsen) F =15.4 ,K =7.46
F =60.2 ,K =29.07
F =31 ,K =14.95
F =2.82 ,K =1
Horizontal buoyant jet in cowflow (Knudsen) F =8.28 ,K =4
F =2.09 ,K =1
F =58.2 ,K =8
F =14.6 ,K =8
JETLAG99
Knudsen
JETLAG2008
Z/D
X/D

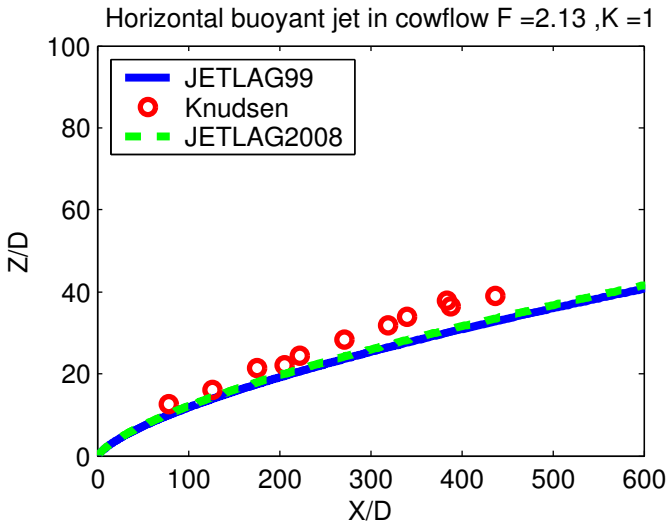

Fig. 10: Comparison of model prediction with data: horizontal buoyant jet in coflow (Knudsen)

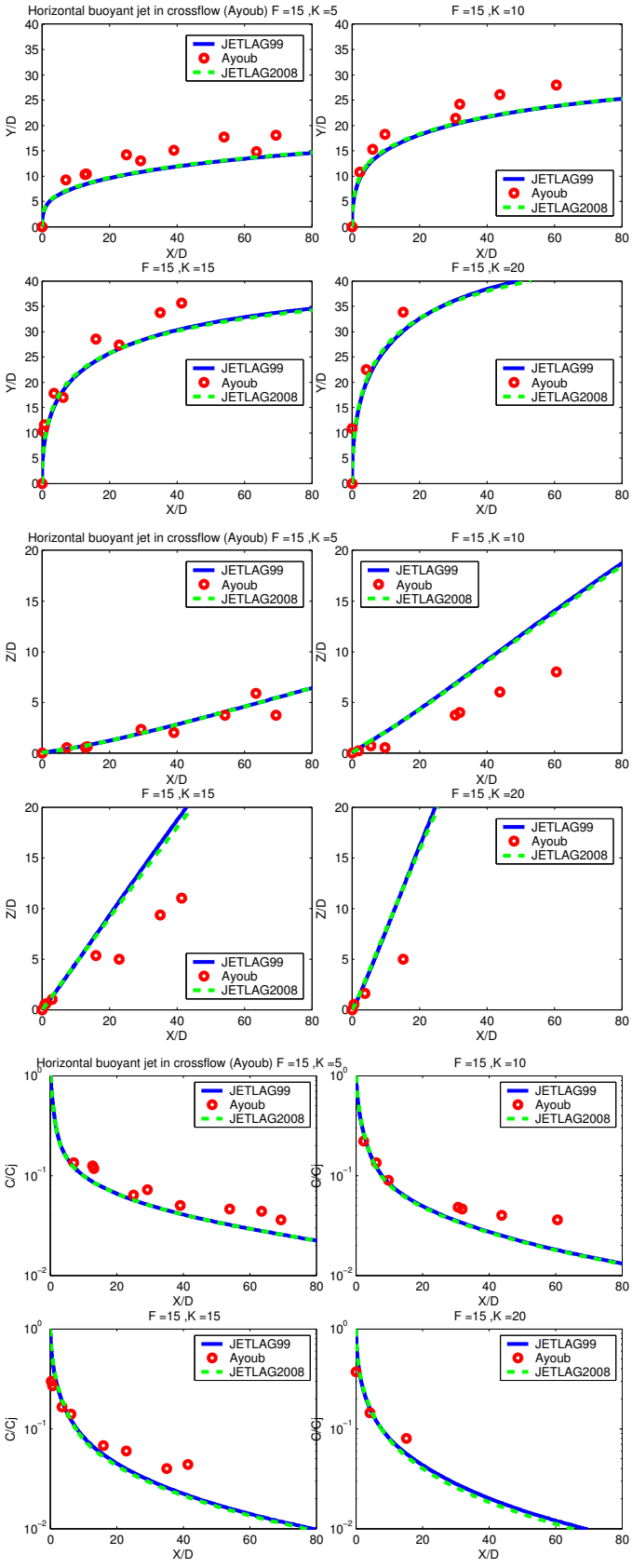
Horizontal buoyant jet in crossflow (Ayoub) F =15 ,K =5
F =15 ,K =10
F =15 ,K =15
F =15 ,K =20
JETLAG99
Ayoub
JETLAG2008
Y/D
Z/D
C/Cj
X/D

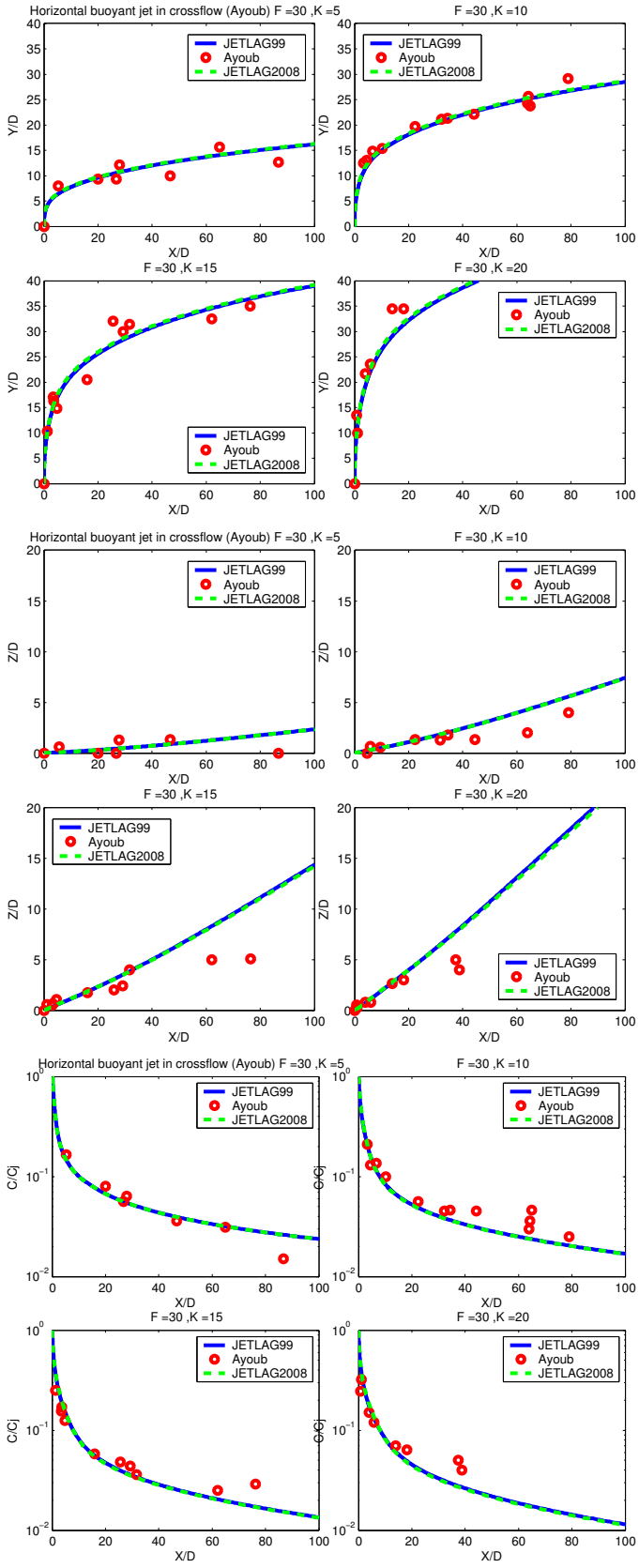
Horizontal buoyant jet in crossflow (Ayoub) F =30 ,K =5
F =30 ,K =10
F =30 ,K =15
F =30 ,K =20
JETLAG99
Ayoub
JETLAG2008
Y/D
Z/D
C/Cj
X/D

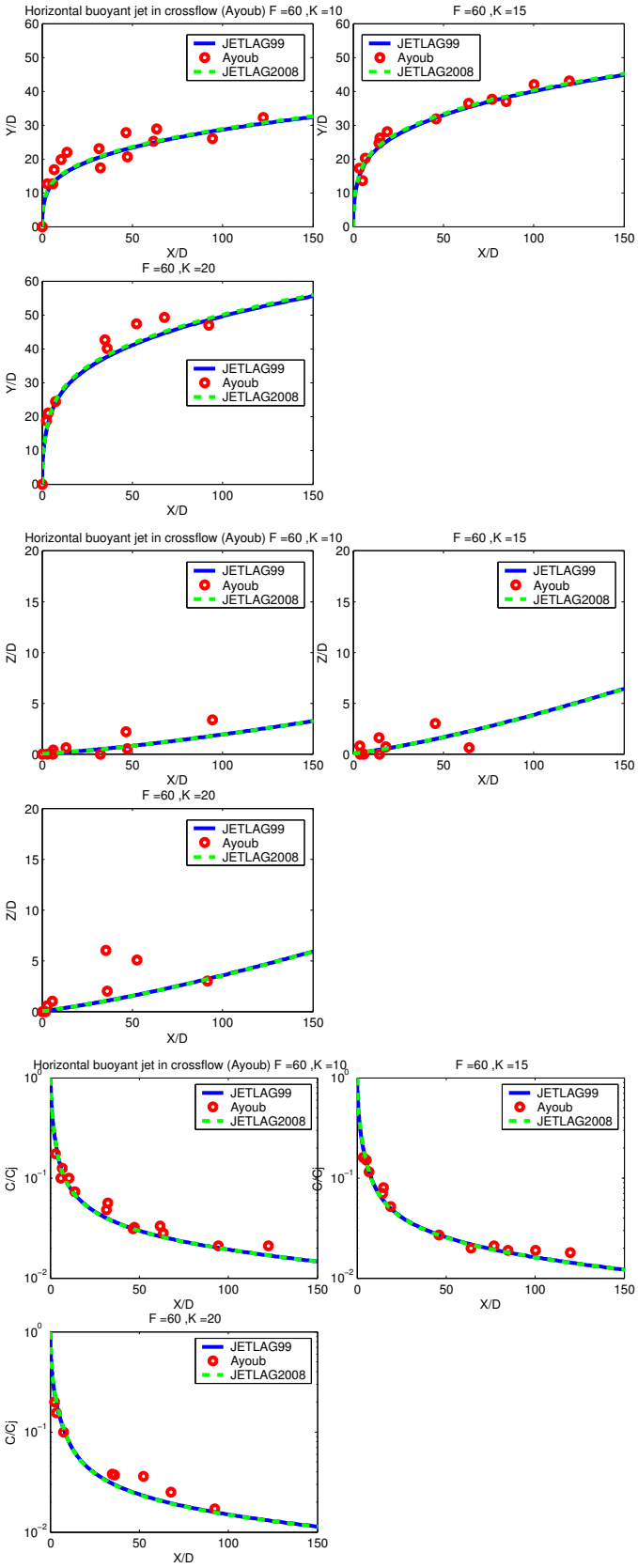
Horizontal buoyant jet in crossflow (Ayoub) F =60 ,K =10
F =60 ,K =15
F =60 ,K =20
JETLAG99
Ayoub
JETLAG2008
Y/D
Z/D
C/Cj
X/D

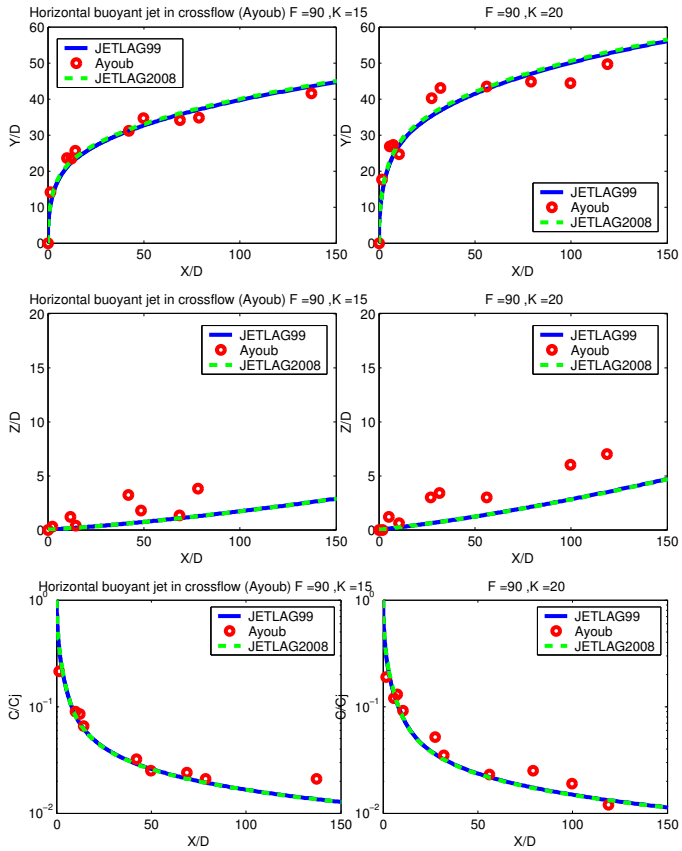

Fig. 11: Comparison of model prediction with data: horizontal buoyant jet in crossflow (Ayoub)

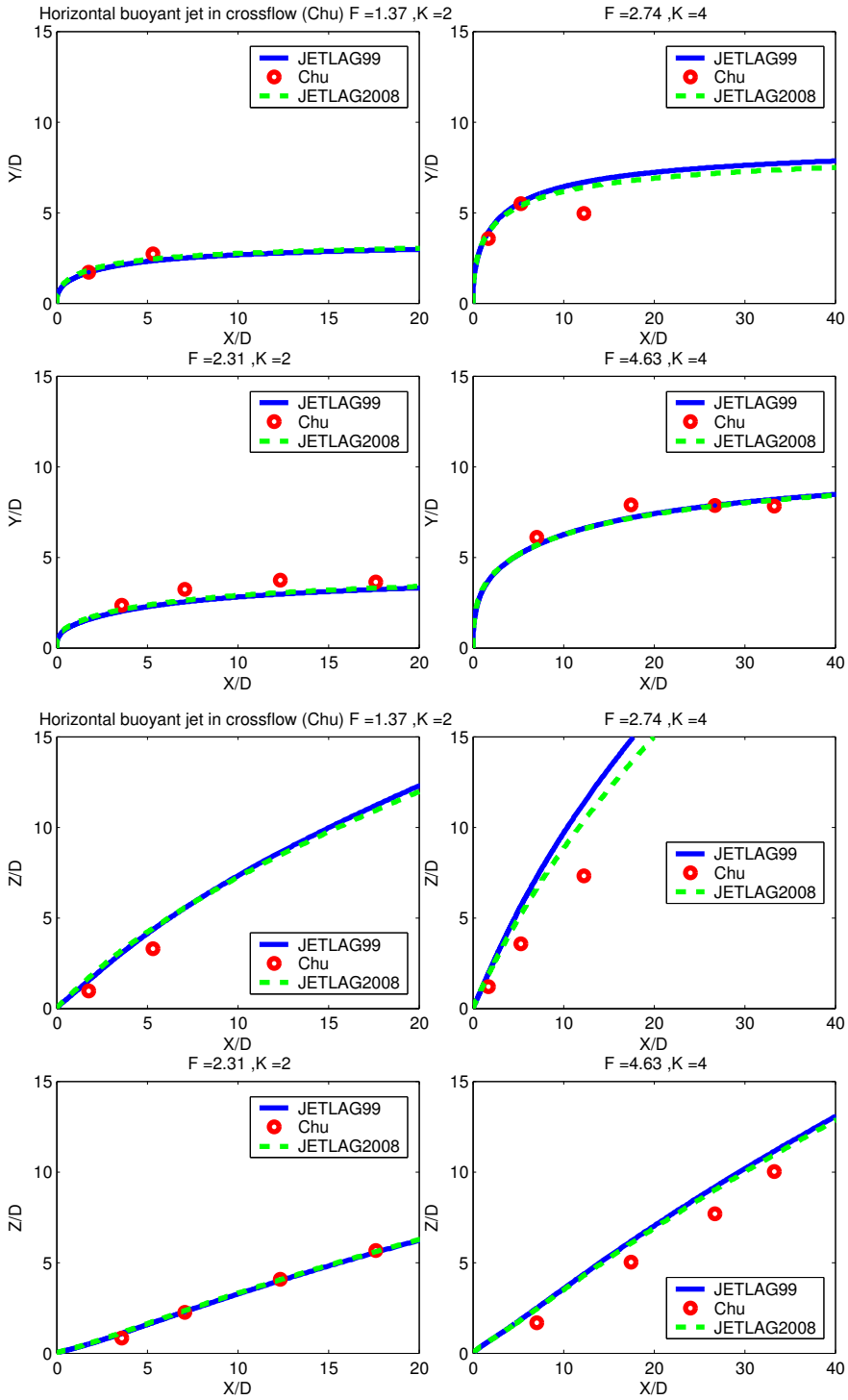
Horizontal buoyant jet in crossflow (Chu) F =1.37 ,K =2
F =2.74 ,K =4
F =2.31 ,K =2
F =4.63 ,K =4
JETLAG99
Chu
JETLAG2008
Y/D
X/D
Horizontal buoyant jet in crossflow (Chu) F =1.37 ,K =2
F =2.74 ,K =4
F =2.31 ,K =2
F =4.63 ,K =4
JETLAG99
Chu
JETLAG2008
Z/D
X/D

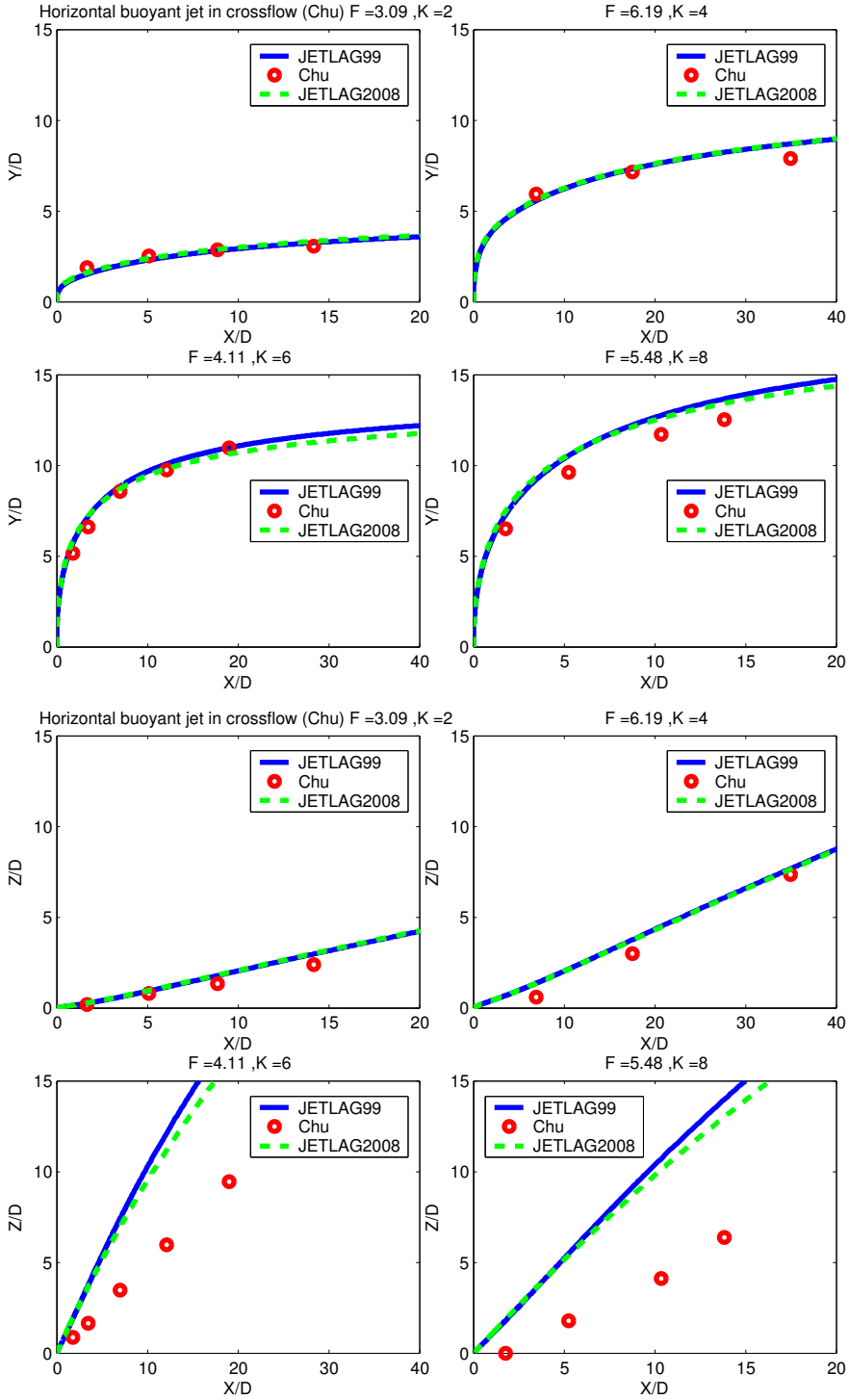
Horizontal buoyant jet in crossflow (Chu) F =3.09 ,K =2
F =6.19 ,K =4
F =4.11 ,K =6
F =5.48 ,K =8
JETLAG99
Chu
JETLAG2008
Y/D
Z/D
X/D

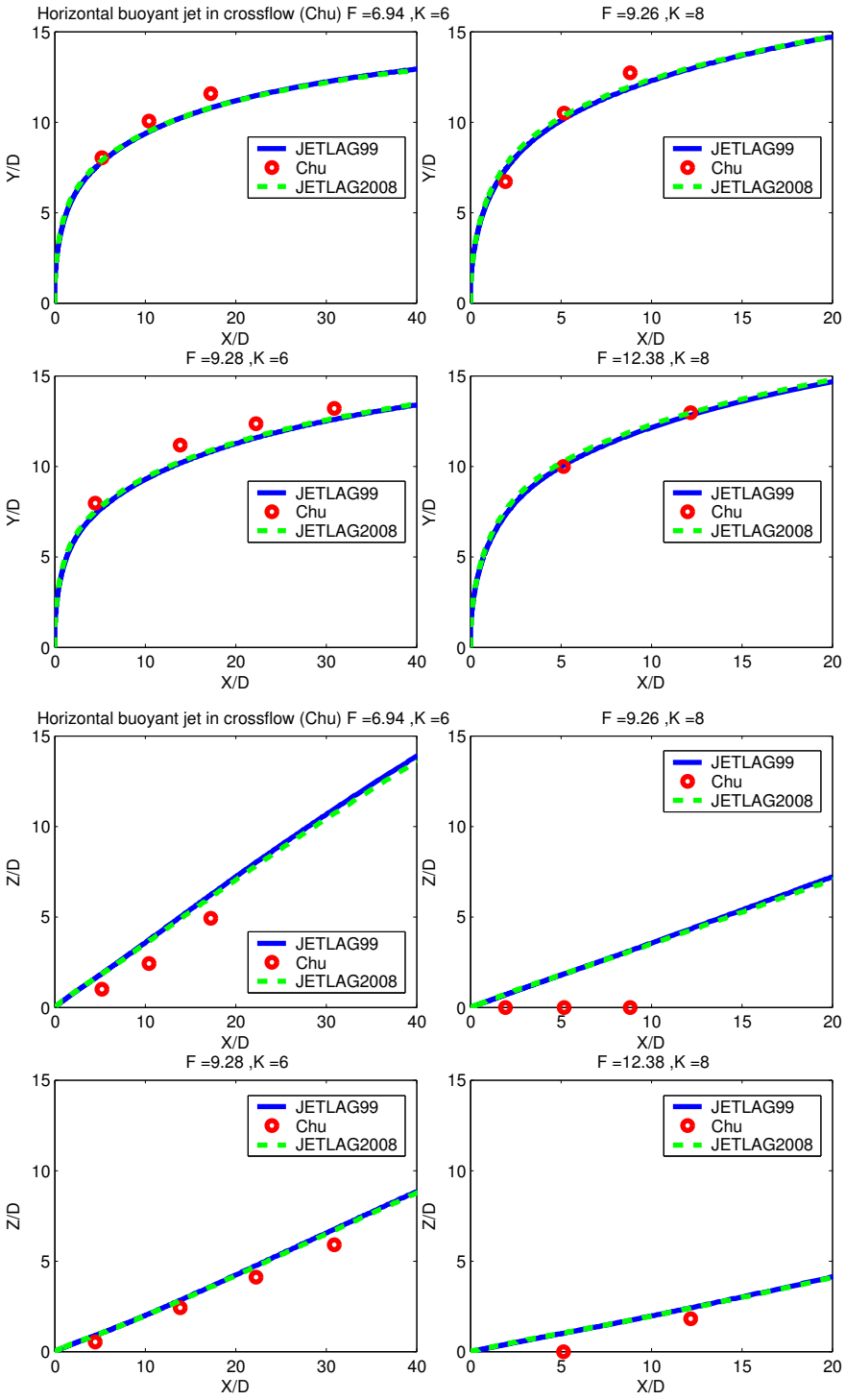

Fig. 12: Comparison of model prediction with data: horizontal buoyant jet in crossflow (Chu)

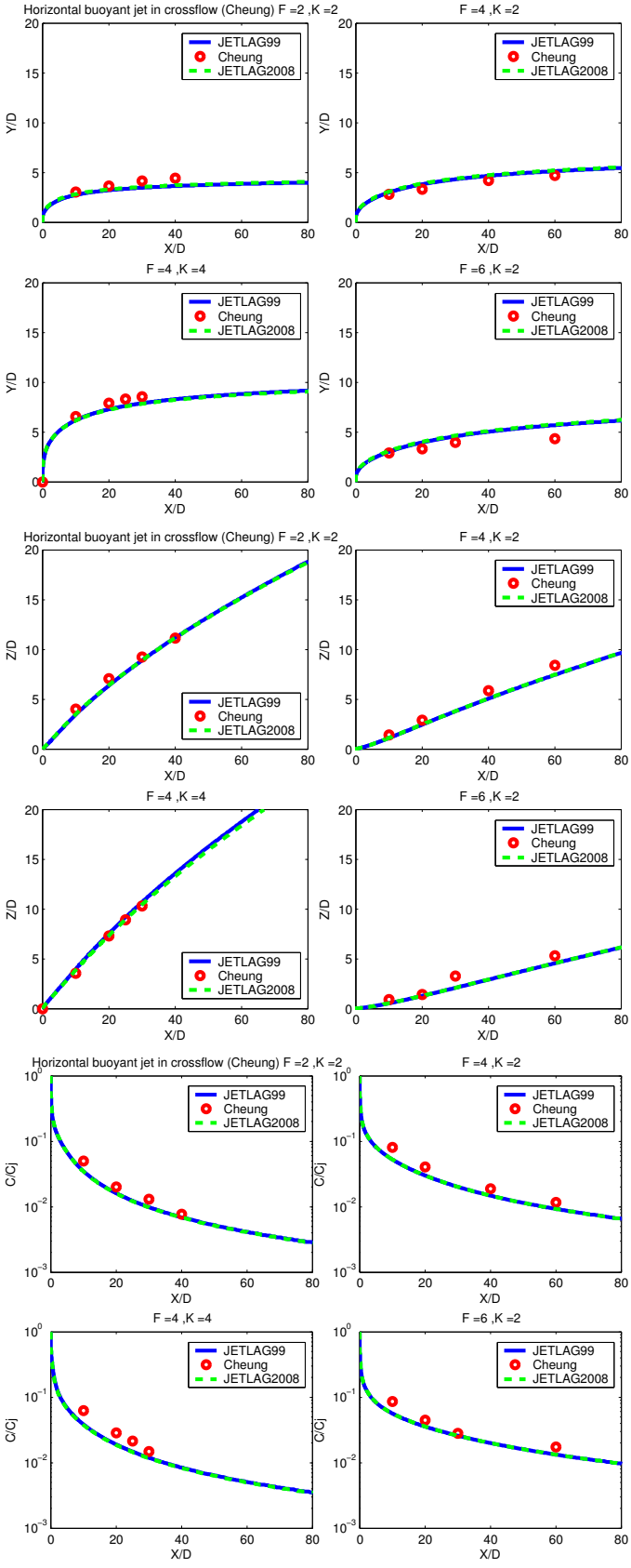
Horizontal buoyant jet in crossflow (Cheung) F =2 ,K =2
F =4 ,K =2
F =4 ,K =4
F =6 ,K =2
JETLAG99
Cheung
JETLAG2008
Y/D
Z/D
C/Cj
X/D

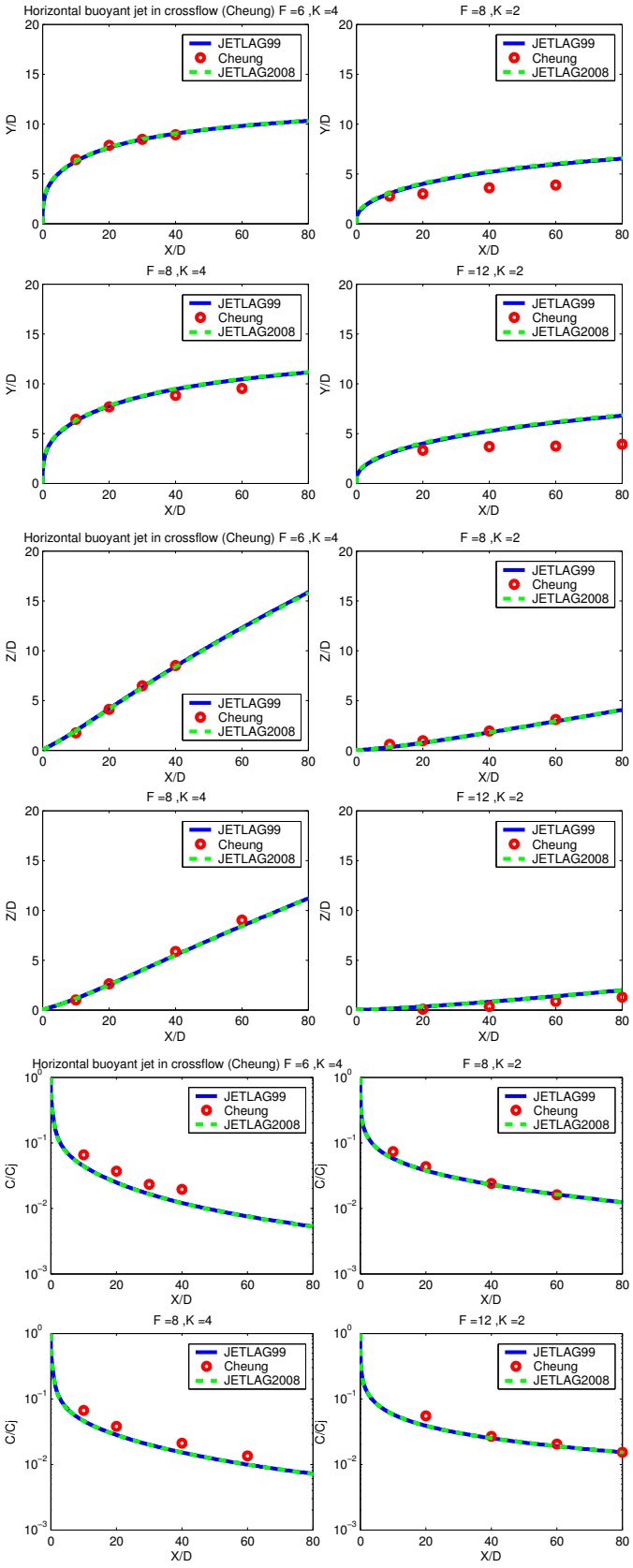
Horizontal buoyant jet in crossflow (Cheung) F =6 ,K =4
F =8 ,K =2
F =8 ,K =4
F =12 ,K =2
Horizontal buoyant jet in crossflow (Cheung) F =6 ,K =4
F =8 ,K =2
F =8 ,K =4
F =12 ,K =2
Horizontal buoyant jet in crossflow (Cheung) F =6 ,K =4
F =8 ,K =2
F =8 ,K =4
F =12 ,K =2
JETLAG99
Cheung
JETLAG2008
Y/D
Z/D
C/Cj
X/D

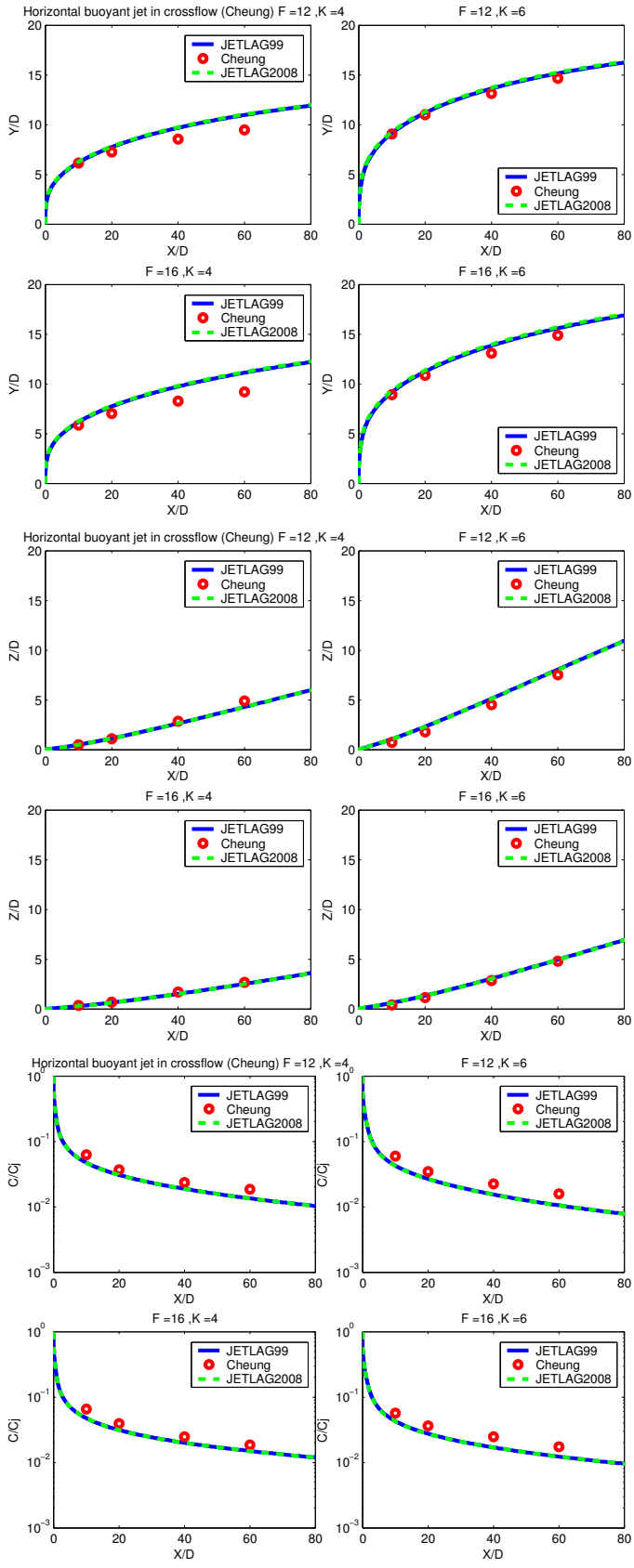

Fig. 13: Comparison of model prediction with data: horizontal buoyant jet in crossflow (Cheung)

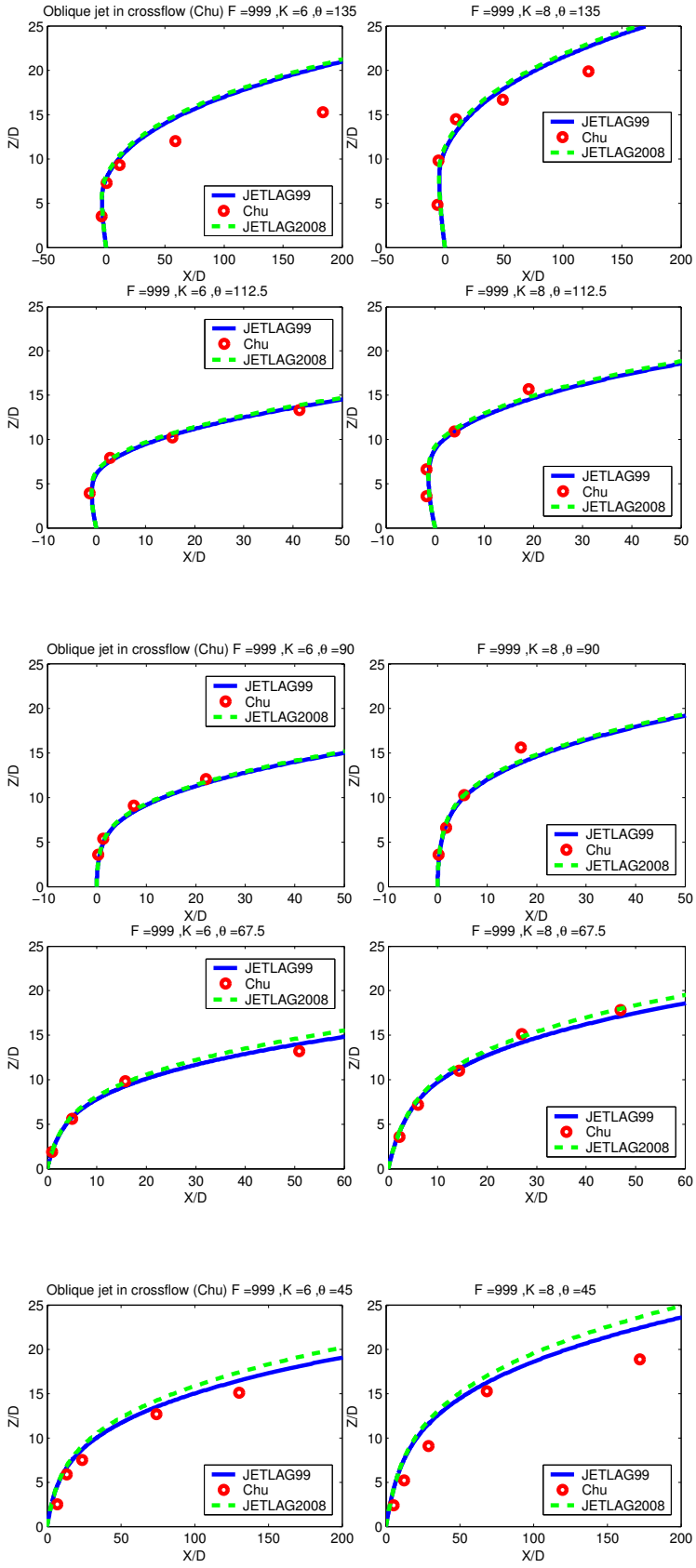

Fig. 14: Comparison of model prediction with data: oblique jet in crossflow (Chu)

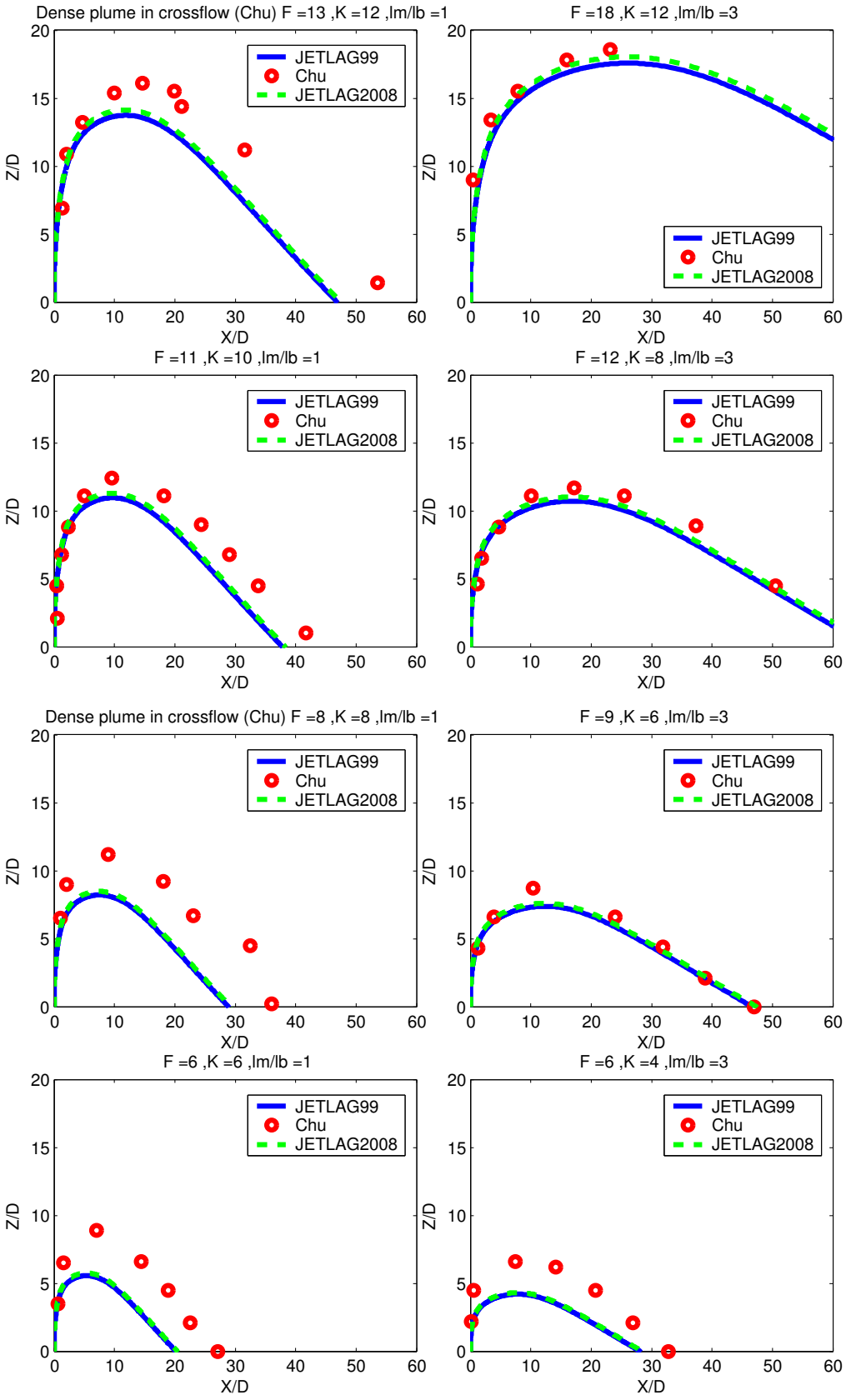

Fig. 15: Comparison of model prediction with data: dense plume in crossflow (Chu)

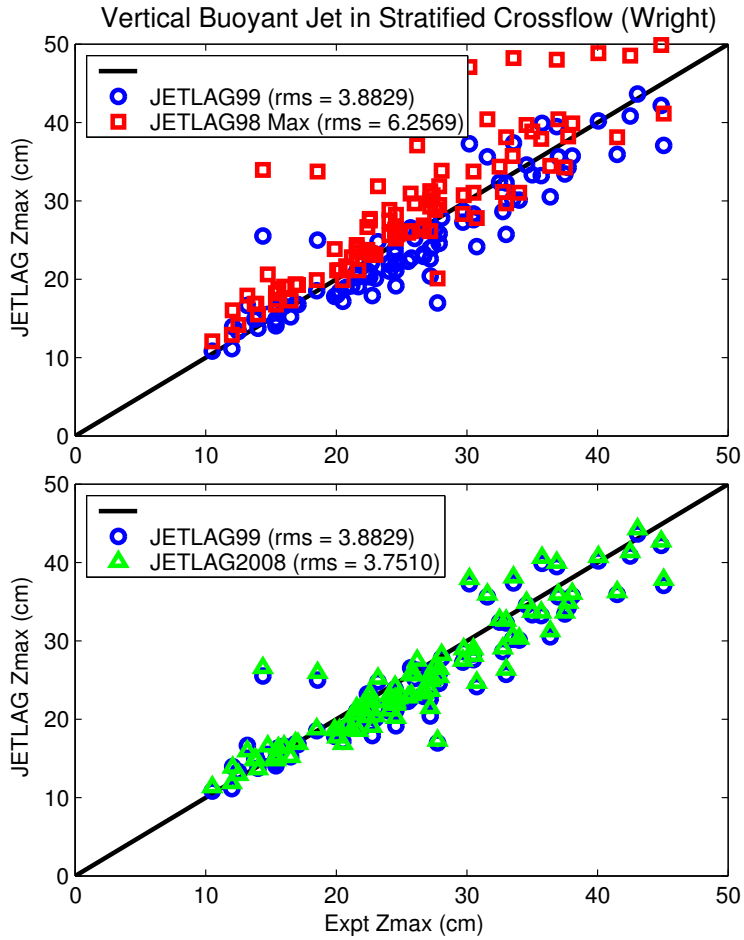
Vertical Buoyant Jet in Stratified Crossflow (Wright)
JETLAG99 (rms = 3.8829)
JETLAG98 Max (rms = 6.2569)
JETLAG Zmax (cm)
JETLAG99 (rms = 3.8829)
JETLAG2008 (rms = 3.7510)
JETLAG Zmax (cm)
Expt Zmax (cm)
0
10
20
30
40
50

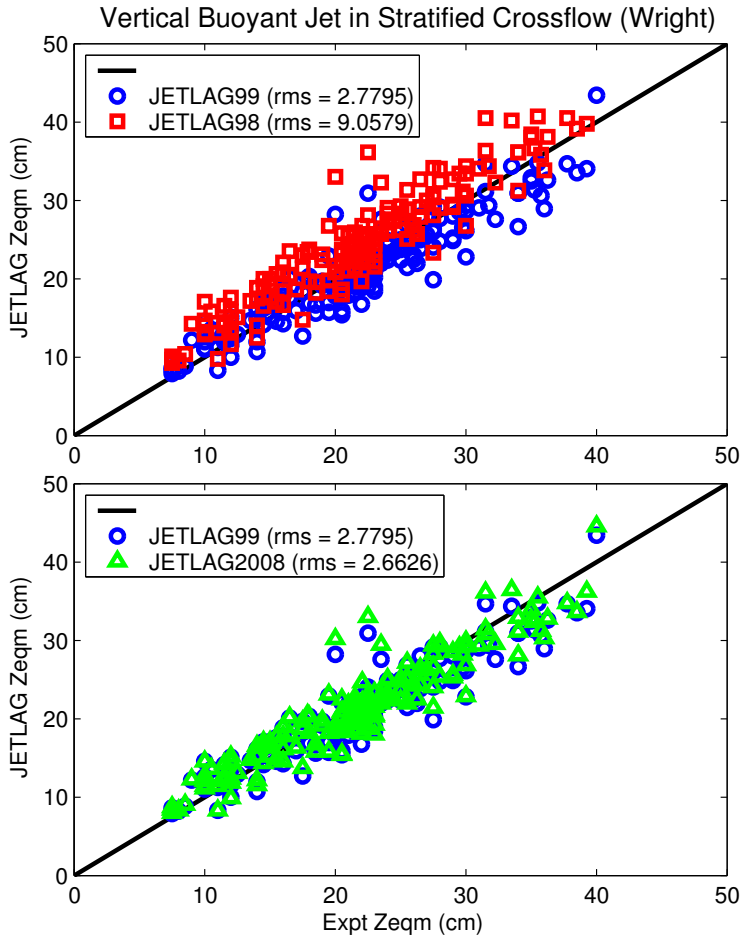

Fig. 16: Comparison of model prediction with data: vertical buoyant jet in stratified crossflow (Wright)

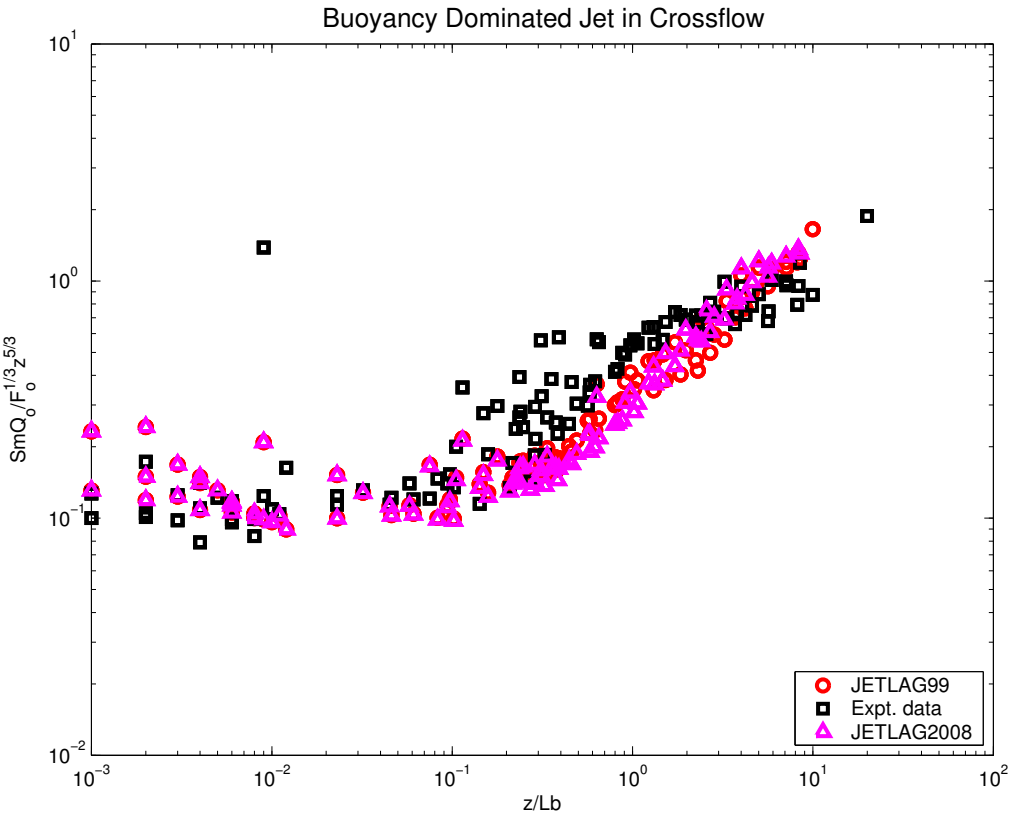

Fig. 17: Comparison of model prediction of centerline dilution with data: vertical buoyant plume in weak crossflow. The dimensionless dilution $S_m Q_o/(F_o^{1/3} z^{5/3})$ is plotted against $z/l_b = z u_a^3/F_o$.

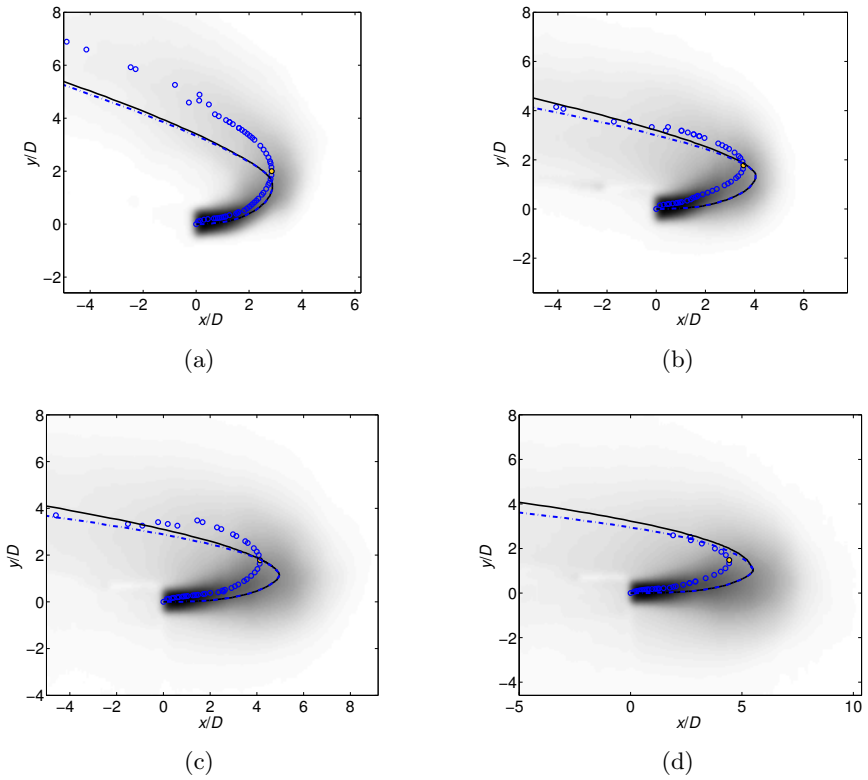

Figure 18: Mean LIF concentration field and JETLAG predicted jet trajectory at $K = u_j/U_a = 2.5$ and different jet densimetric Froude number F: (a) F=3; (b) F=5; (c) F=7.5; (d) F=10. JETLAG 1999 (black solid line); JETLAG 2008, with transition $f(\phi) = \tanh[6(\frac{\pi}{2} - \phi)]$ (blue dash-dot line); symbols: image processing.

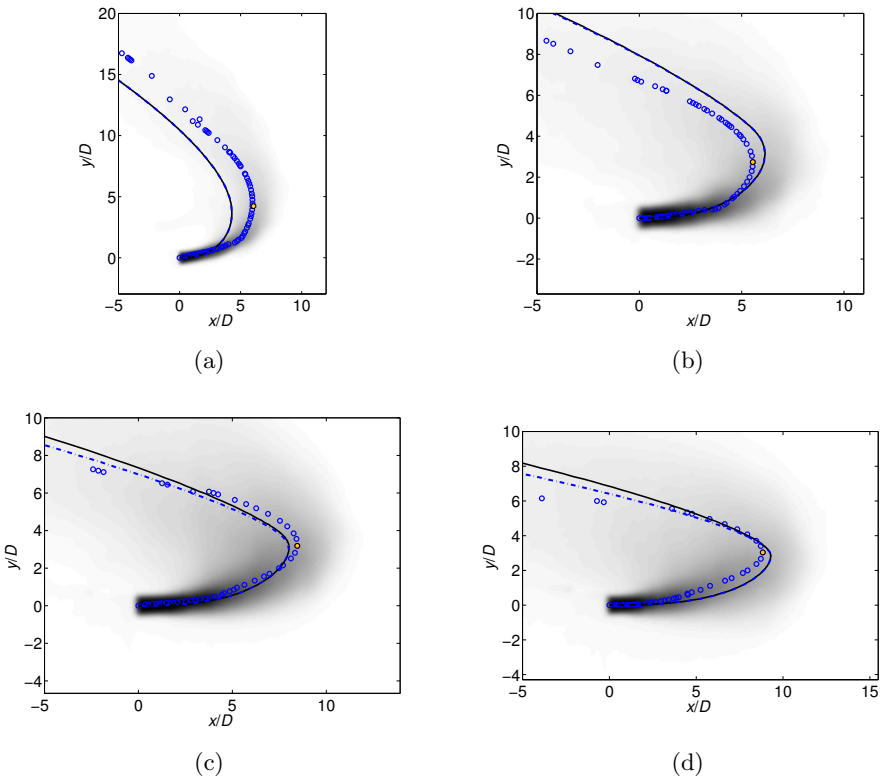

Figure 19: Mean LIF concentration field and JETLAG predicted jet trajectory at $K = u_j/U_a = 5$ and different jet densimetric Froude number F: (a) F=3; (b) F=5; (c) F=7.5; (d) F=10. JETLAG 1999 (black solid line); JETLAG 2008, with transition $f(\phi) = \tanh[6(\frac{\pi}{2} - \phi)]$ (blue dash-dot line); symbols: image processing.

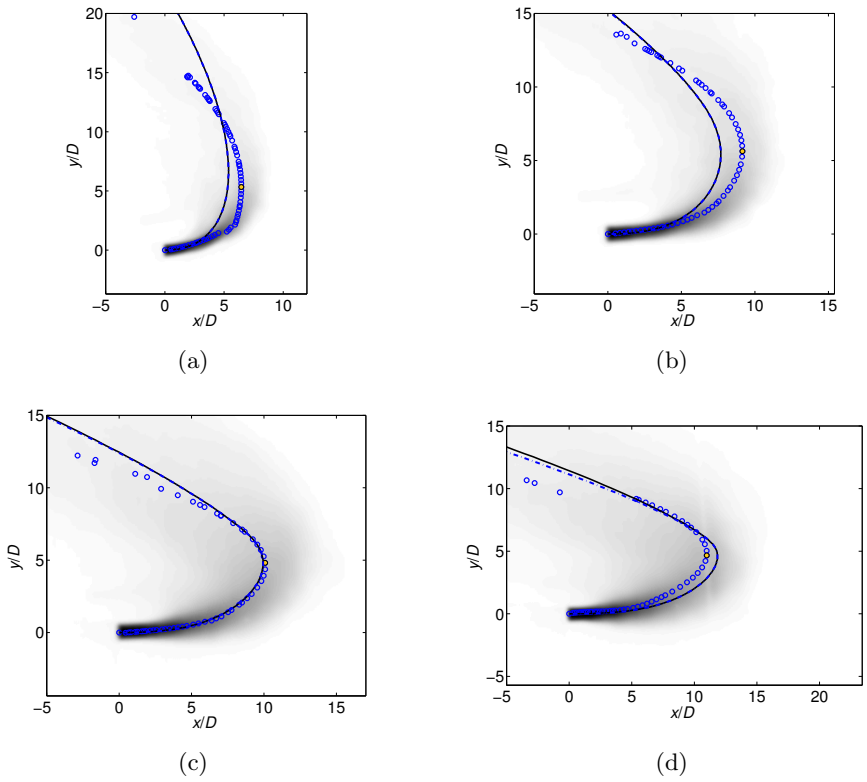

Figure 20: Mean LIF concentration field and JETLAG predicted jet trajectory at $K = u_j/U_a = 7.5$ and different jet densimetric Froude number F: (a) F=3; (b) F=5; (c) F=7.5; (d) F=10. JETLAG 1999 (black solid line); JETLAG 2008, with transition $f(\phi) = \tanh[6(\frac{\pi}{2} - \phi)]$ (blue dash-dot line); symbols: image processing.

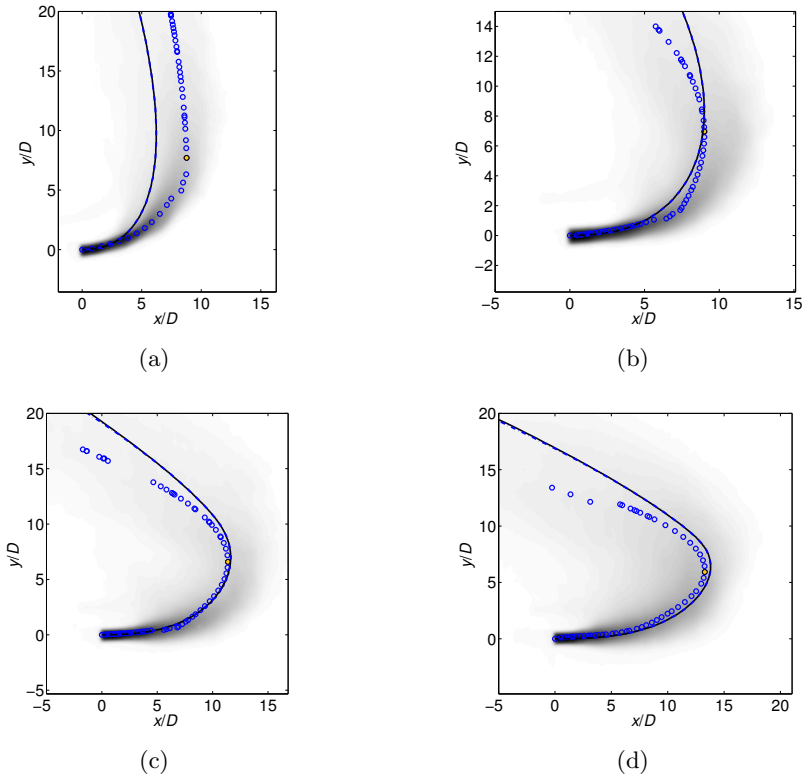

Figure 21: Mean LIF concentration field and JETLAG predicted jet trajectory at $K = u_j/U_a = 10$ and different jet densimetric Froude number F: (a) F=3; (b) F=5; (c) F=7.5; (d) F=10. JETLAG 1999 (black solid line); JETLAG 2008, with transition $f(\phi) = \tanh[6(\frac{\pi}{2} - \phi)]$ (blue dash-dot line); symbols: image processing.

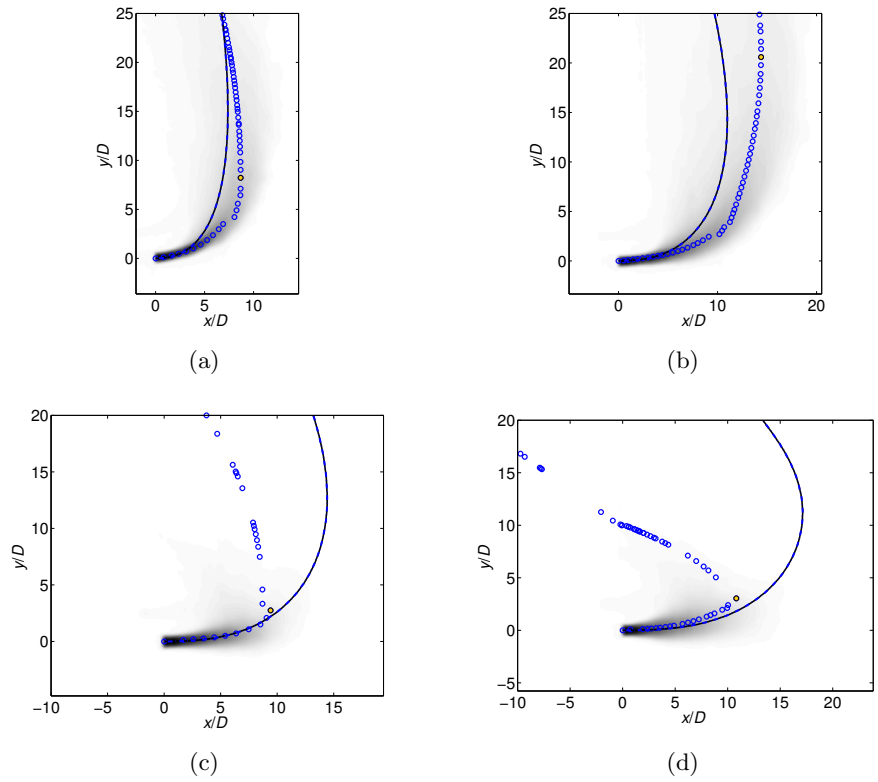

Figure 22: Mean LIF concentration field and JETLAG predicted jet trajectory at $K = u_j/U_a = 15$ and different jet densimetric Froude number F: (a) F=3; (b) F=5; (c) F=7.5; (d) F=10. JETLAG 1999 (black solid line); JETLAG 2008, with transition $f(\phi) = \tanh[6(\frac{\pi}{2} - \phi)]$ (blue dash-dot line); symbols: image processing.

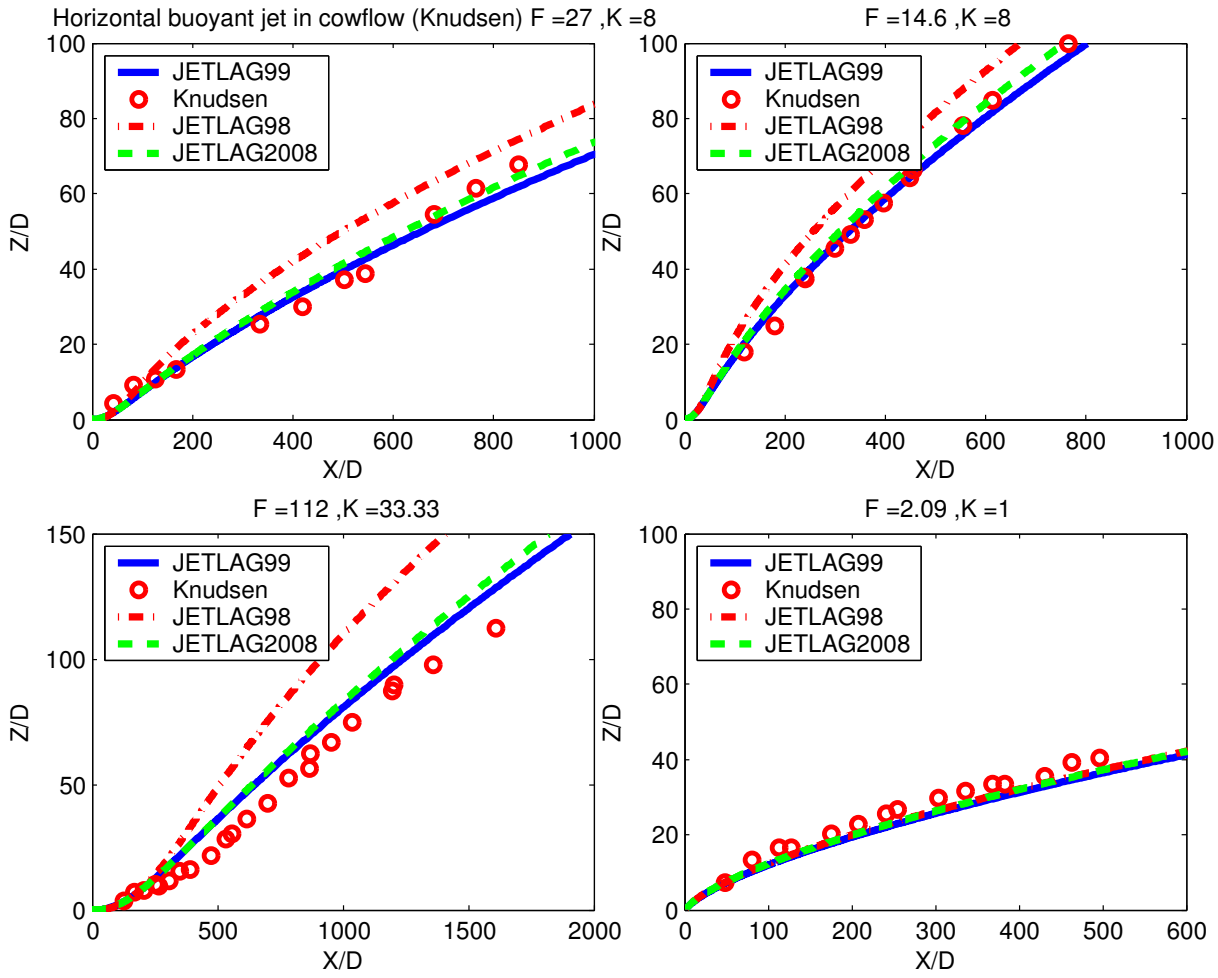

Fig. 21: Horizontal Jet in Coflow (Knudsen) - comparison of different model predictions with data

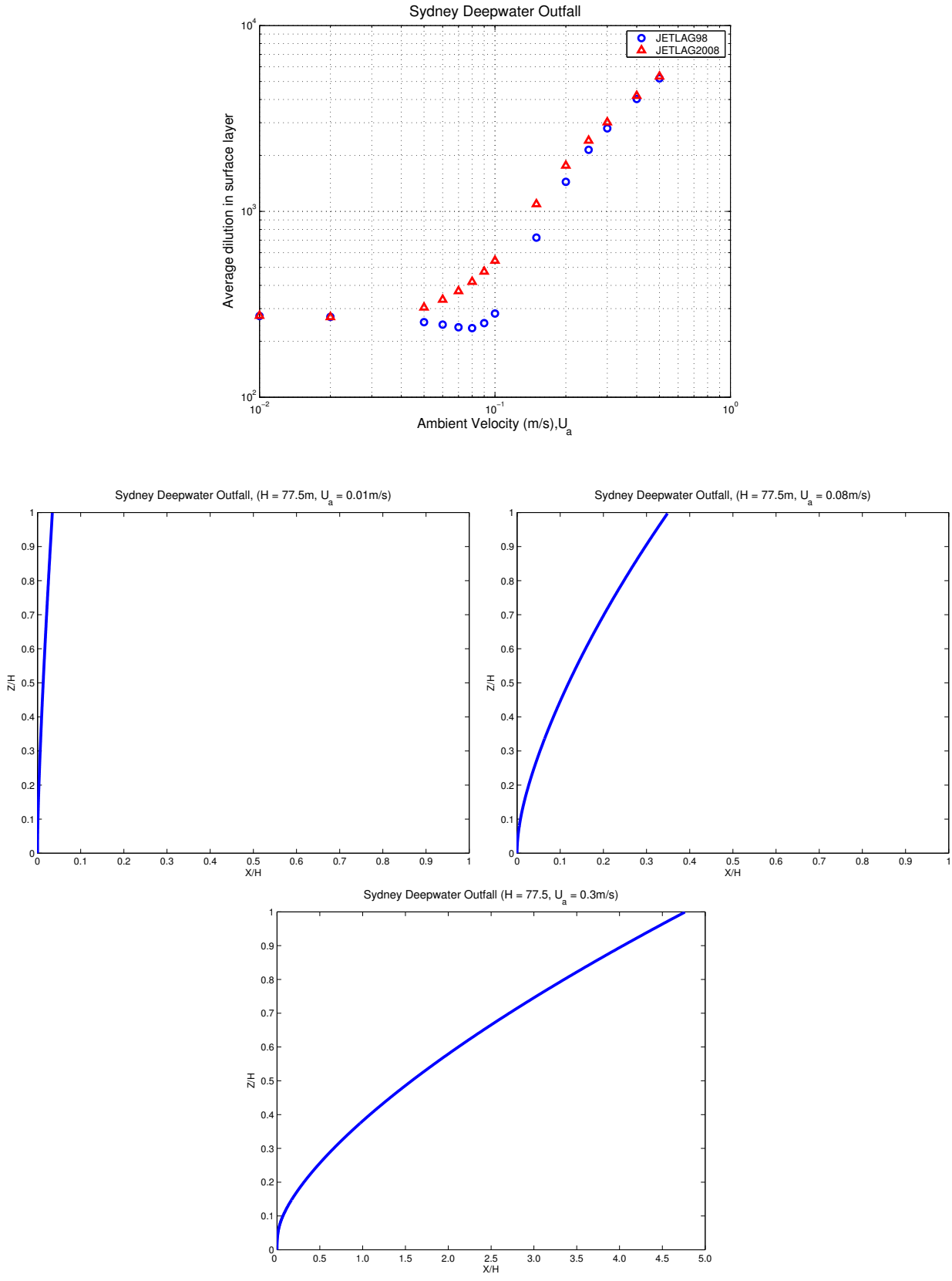

Fig. 22: Vertical Buoyant Plume in a Crossflow: (a) variation of surface dilution with current speed (top); (b) predicted plume trajectory for $u_a = 0.01, 0.08, 0.3$ m/s (bottom)

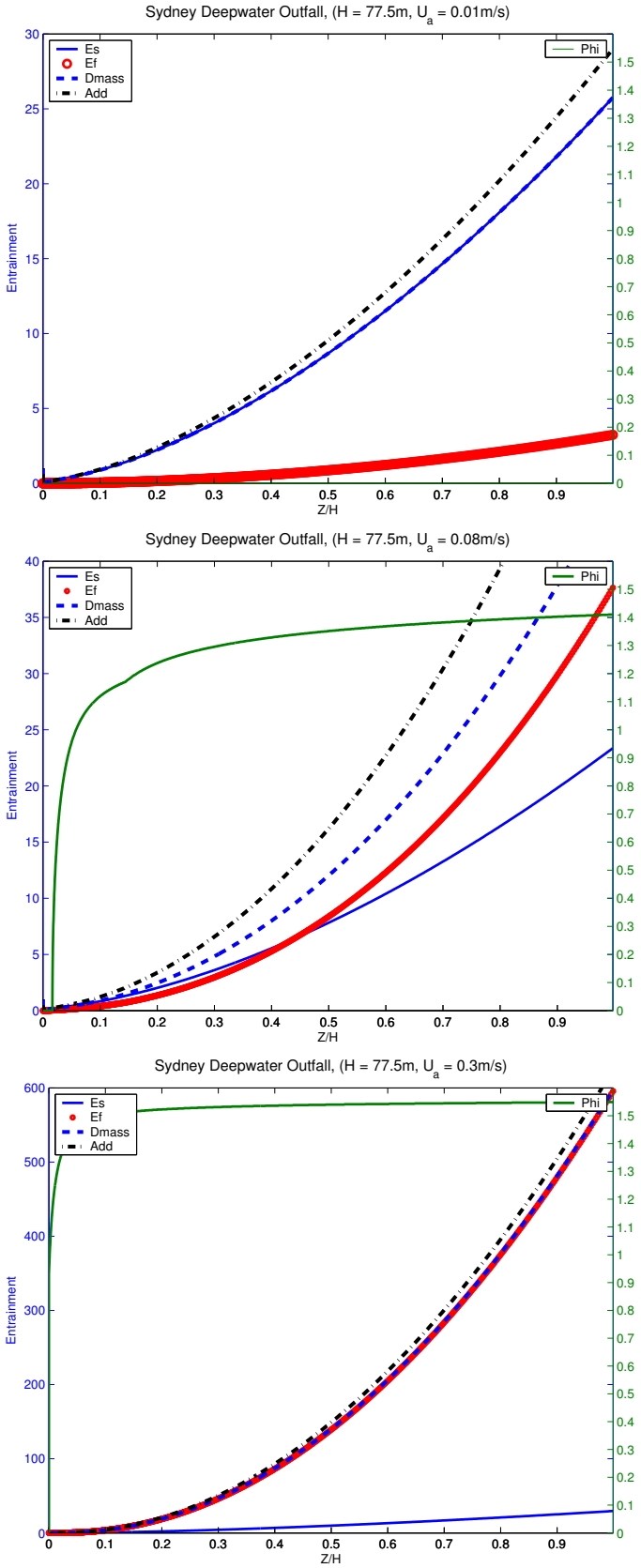

Fig. 23: Vertical buoyant plume in crossflow: variation of separation angle, shear entrainment (E_s), vortex entrainment (E_f) and total entrainment (DMass) along the jet trajectory; additive hypothesis also shown.